Application of phase change materials to enable the cold weather operability of B100 in diesel trucks

by

Obiajulu Nnaemeka

A Thesis Submitted to the Faculty of Graduate Studies of
the University of Manitoba
in Partial Fulfilment of the Requirements of the Degree of

MASTER OF SCIENCE

Department of Mechanical Engineering
The University of Manitoba
Winnipeg, Canada

Abstract

The use of B100 biodiesel for compression ignition engines during the winter poses a challenge due to gelling and plugging of engine filters and fuel lines. The most common method to prevent this issue is blending it with petroleum diesel and many engine manufacturers limit the biodiesel in blends to 20% or less for warrantee purposes; as low as 5% may be set for winter months. In this research, an experimental analysis is performed using a scaled model of the fuel tank with canola oil as a test fluid in the tank. The tank is subjected to an ambient temperature of −20°C in an icing tunnel facility with air velocity at 10 m/s. The results show that the time for the oil to drop from 20°C to 5°C was increased from 18.6 hours to 22.5 and 33 hours respectively when 4 and 12 tubes containing phase change materials (PCM) were inserted in the tank containing 33 litres of canola oil. A numerical model was further formulated to predict the transient temperature of the oil and comparison with experimental results showed excellent agreement. ANSYS Fluent was then used to conduct a visualization study of the flow for a sample scenario of a commercial tank with PCM. Finally, the developed numerical model was used to simulated different cases to investigate the effect of tank filling level, overall heat transfer coefficient, number of PCM modules and diameter of PCM modules on the tank performance. Results show that B100 can be implemented in diesel engines in cold climates.

Acknowledgements

I specially thank my Research Advisor, Dr. Eric Bibeau for giving the opportunity to conduct this research as part of his research group. I sincerely admire and respect his passion and commitment to the development of renewable energy and share in his vision for a greener and better future. I also thank members of the examining committee, Dr. Vijay Chatoorgoon and Dr. Stefan Cenkowski for their time in reviewing my thesis and the very important feedbacks I received to further develop this work. I acknowledge the invaluable support of Zeev Kapitanker, who guided me all the way from the design part of my work to the final fabrications and trained me in using the lab equipment needed to carry out the experimental work. My peers at the Renewable Energy Research Group were also vital to make this project a reality by creating a respecting, exciting and supportive work environment. This work would also not have been possible without the financial support from the University of Manitoba (UMGF and IGSES), Government of Manitoba (MGS), NSERC Discovery grant, and the GETS funding.

Finally, I thank my parents, Mr. & Mrs. Nnaemeka, and my siblings for their continuous prayers and support all the way from Nigeria. I love you all from the bottom of my heart!

Contents

List of Tables

List of figures

Nomenclature

English symbols

A	Surface area (m^2)
C	Mushy zone parameter
C_p	Specific heat capacity (J/kgK)
dr	Radial distance between two nodes (m)
f	Liquid fraction
g	Gravitational acceleration (m/s^2)
h	Enthalpy (J/kg)
h_{pcm}	Heat transfer coefficient on PCM tube (W/m2K)
H_{pcm}	Wetted height of PCM tube (m)
k	Thermal conductivity (W/mK)
L	Latent energy (J/kg)
m	Mass (kg)
Nu	Nusselt number
p	Pressure (N/m^2)
Pr	Prandtl number
$\dot{Q}$	Heat transfer rate (W)
R	Thermal resistance (m^2K/W)
Ra	Rayleigh number
$\boldsymbol{S}$	Momentum source term
T	Temperature (K)
t	Time (hr)
$\boldsymbol{u}$	Velocity vector (m/s)
U	Overall heat transfer coefficient (W/m^2K)
V	Volume (m^3)
w	Grid weight (m)

Greek symbols

Δ	Difference
ε	Small number to prevent division by zero
∇	Differential operator
ρ	Density
μ	Dynamic viscosity

Subscripts

amb	Ambient
b	Bottom
con	Container
$cond$	Conduction
$conv$	Convection
d	Decay
e	External
eff	Effective
i	Internal
in	Intermediate phase
ins	Insulation
int	Interface
k	n^{th} node
l	Liquid phase
n	Number of nodes
$n+1$	Container node
pcm	As regards phase change material
s	Free surface
so	Solid phase

st	Oil storage
w	Wall

Superscripts

1	Initial
2	Final
t	Previous time step
$t + 1$	Present time step

1

Background

1.1 Global energy scenario

The world population is estimated to increase to 9.9 billion by the year 2050, a rise of 33% from the recently published figure of 7.4 billion in 2016 [1]. Rapid industrialization and better standards of living coupled with the projected population growth will inevitably place a corresponding rise in the global energy consumption. Future global energy consumption will primarily depend on development in technology, demographic changes, economic trends and availability of resources that drive energy use. The U.S Energy Information Administration projects that the global energy consumption will increase to 736 Quadrillion BTU (216 PWh) in 2040, up 28% from the figure of 575 Quadrillion BTU (169 PWh) in 2015 [2]. A significant portion of this increase will be from the Non- Organization for Economic Co-operation and Development (Non-OECD) nations due to strong economic growth, increased population and increased access to the energy market as shown in Figure 1.1.

Currently, fossil fuel accounts for over 85% of the global primary energy consumption and there is growing concern about its environmental impact and future sustainability [3]. In 2016, the United States Environmental Protection Agency (EPA) reported the CO_2 concentration in the atmosphere as 401 ppm, up 43% from an annual average of 280 ppm in the late 1700s [4]. We are thus entering an era where anthropogenic CO_2 will decisively impact all aspects of life. CO_2 concentrations may be rising further due to our increased dependence on fossil fuels—surpassing the critical 500 ppm in the next few decades may be inevitable. Increasing the share of renewables in the energy sector, increasing the efficiency of power producing systems and reducing energy demands are ways in which the global renewable energy ratio can be increased with the aim of saving our planet.

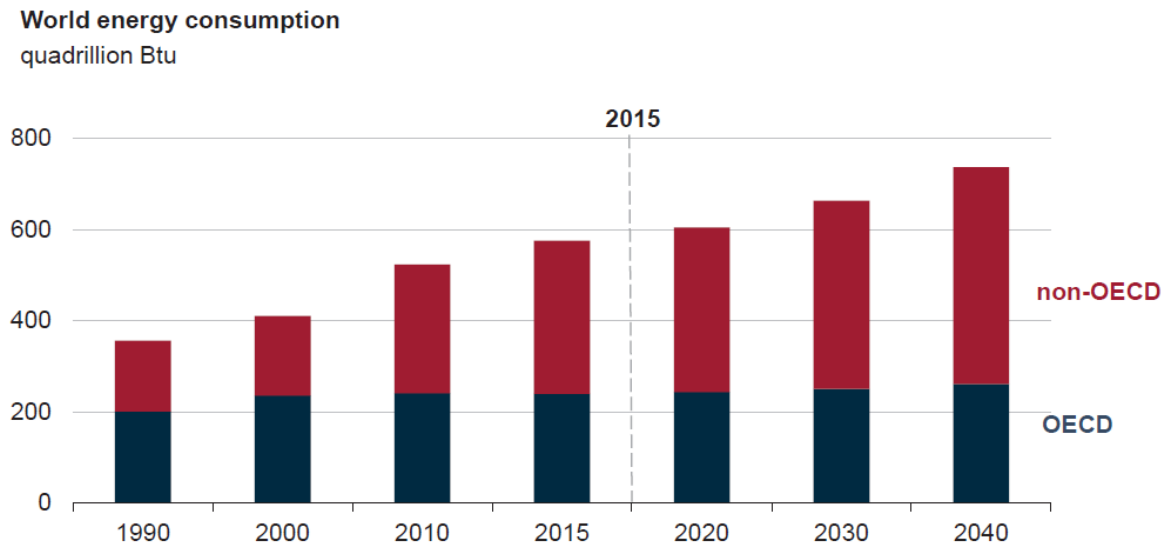

Figure 1.1: Past and projected global energy consumption from 1990 – 2040 [2]

1.2 Renewable fuels

The global rise in energy consumption discussed in the previous section will result in inevitable issues of energy security and environmental sustainability if the increased energy demand is not addressed accordingly. Peak oil production and subsequent exhaustion of reserves in high energy consuming countries like the US, China and India few decades from now will place huge pressure on the oil exporting countries, resulting in their reserves even depleting at a much faster rate. Proactive measures should be taken by government around the world to avert this impending crisis, especially in developing countries where population growth rate is relatively higher and there are more opportunities to diversify the energy mix due to economic growth.

About 50% of the world oil production is utilized by the transportation sector and it accounts for about 25% of global fuel CO_2 emissions [5]. With the growing concern about greenhouse gas (GHG) emissions and fossil fuel depletion, there is imminent need to develop alternative energy sources and technologies. Renewable fuels present a potential to reduce the amount of GHG emission in the transportation sector and guarantee future energy security. Bioethanol and biodiesel, also regarded as biofuels, are the most commonly used renewable fuels today and blends with petroleum fuels of up to 85% and 20% respectively remains widely commercialized in the EU, Brazil and United States [6]. There exists an opportunity to increase the share of renewables in the transportation sector by encouraging higher blends of biofuels, however, the debate on whether biofuels can significantly displace the use of fossil fuels continues; being fuelled by topics on economic viability, fuel compatibility with existing

technologies, environmental considerations and food scarcity. These to a large extent has negatively influenced government policies on the use of biofuels in many countries. Further research needs to be done on biofuels to quell some of these debate topics.

Over the past decade, the retail price of biodiesel has been higher than that of petroleum diesel. The higher cost is due to the higher processing cost and low supply of the product. There are not so many existing biodiesel refineries and the few which are available produce at a smaller scale compared to petroleum diesel due to lower demand. Demand for B100 biodiesel is currently primarily for blending with diesel fuel. Producing in smaller scale makes the economics unfavourable and less attractive to potential investors.

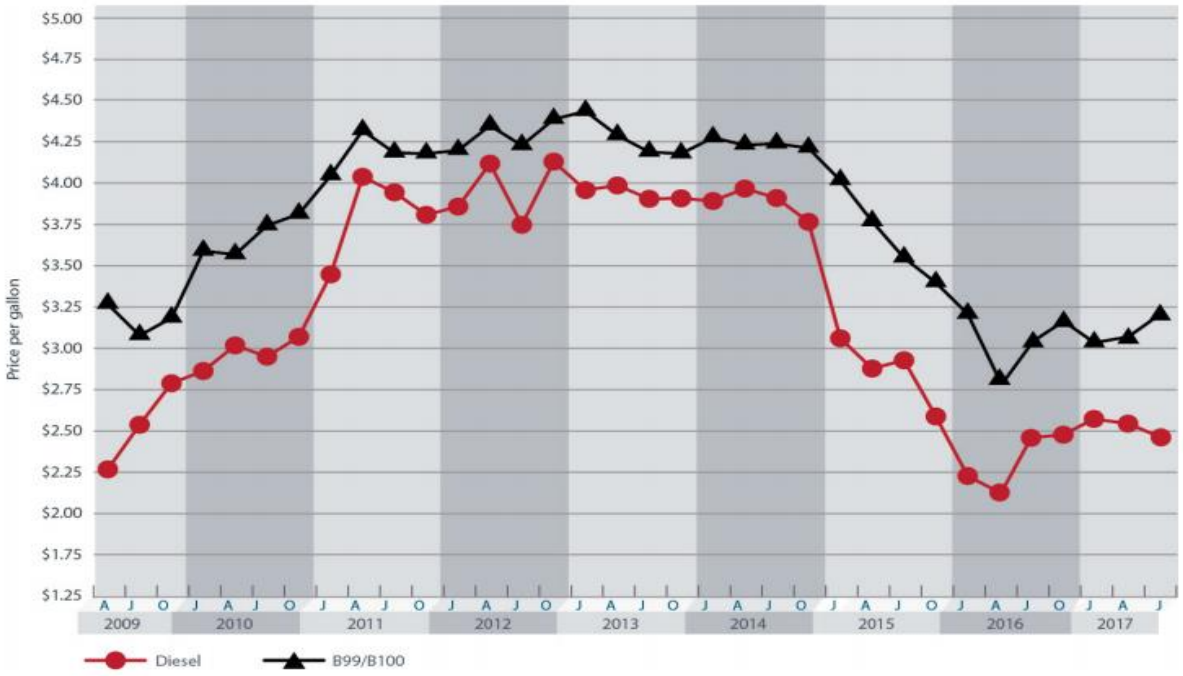

Figure 1.2: Cost of petroleum diesel and biodiesel from 2009 – 2017 [7]

As at July 2017, the national average price of B100 biodiesel in the United States, which is the global leading producer of biodiesel was $3.15 per US gallon while that of petroleum diesel was $2.20 [7]. Figure 1.2 shows the trend of the prices of petroleum diesel and biodiesel from 2009 to 2017. With advancement in technology and production processes, for example, by utilizing consolidated bioprocessing or increasing the yield of algae for biodiesel production, it is expected that the cost of production of biofuels would decline in the coming years and enable greater competition in the energy market without any subsidy or incentive from the government.

1.3 Problem statement

Biodiesel is the generic name for variety of long chain (16-24 carbon atoms) ester-based oxygenated fuels derived from biological sources. According to ASTM D6751 [8], biodiesel is composed of mono-alkyl esters of long-chain fatty acids derived from plant oils and animal fats [9]. Biodiesel is made from the transesterification reaction which involves chemically reacting triacylglyerides (TAG) with an alcohol with the aid of an acidic or basic catalyst. Methanol or ethanol is frequently used in this process. The product of the transesterification reaction is glycerol and three fatty acid alkyl esters as shown in Figure 1.3. When methanol is used, the resulting biodiesel is popularly known as fatty acid methyl ester (FAME).

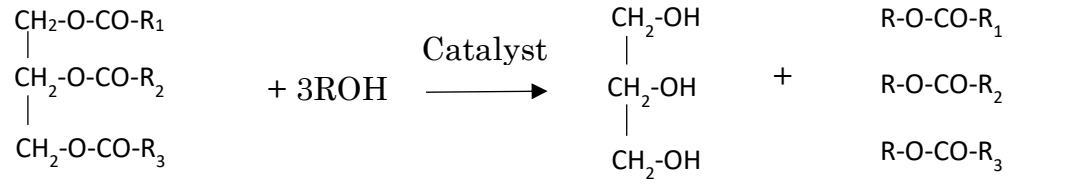

Triglyceride Alcohol Glycerol Fatty acid alkyl esters

Note: R represents the alkyl groups

Figure 1.3: Transesterification reaction which produces glycerol and biodiesel

TAG is derived from a variety of feedstock which can be categorized into edible (first generation), non-edible (second generation) or algae (third generation) sources. FAME produced from the transesterification process have similar combustion properties to that of petroleum diesel and can be alternatively used in diesel engines without the need of any modifications, just like the first diesel engine designed by Dr. Rudolf Diesel in the late 19th century which ran on vegetable oil. However, it poses a great problem in cold weather due to the unique stacking of its saturated hydrocarbon molecules which causes crystallization and gelling and negatively affects its flow properties. The ultimate result of this is plugged filters and fuel starvation when used in compression-ignition engines.

Despite the bad performance of biodiesel in cold weather, there are several advantages of using them in place of petroleum diesel. These are outlined below:

i. Biodiesel is a renewable fuel since it produced from renewable sources such as plant oils or animal fat.

ii. It can be used to displace petroleum diesel in existing compression ignition engines. Performance of biodiesel is very similar to that of petroleum diesel and their energy content is only 12.5% lower than petroleum diesel per pound [9]. Biodiesel can also be blended with petroleum diesel and used in most diesel equipment with little or no modifications.

iii. It reduces GHG emissions. Biodiesels can be classified as carbon neutral since their resulting CO_2 emission from the process of combustion is used as plant food for conversion into biomass. This carbon cycle continues over many decades resulting in a net-zero addition to the CO_2 concentration in the atmosphere.

iv. Biodiesels are non-toxic and biodegradable. Also, due to their very minimal particulate matter emission they are suitable for use in very sensitive environments or in conditions were emissions from petroleum diesel pose a health risk.

v. Engine operation is improved by using biodiesel. This is because the use of biodiesel improves lubricity which is good for preventing moving parts in the engine like the fuel pumps from wearing. Even in blends as low as 1% of biodiesel they can provide adequate lubricity to diesel fuels [9].

1.4 Objectives of research

Considering the problem of using biodiesel in cold weather as highlighted in the previous section, the objectives of this research are outlined as follows:

i. To investigate experimentally and numerically, the benefits of implementing phase change materials (PCM) in heavy duty truck fuel tanks to enable the cold weather operability of B100 during the winter periods.

ii. To determine a B100 biodiesel tank design and PCM configuration for suitable for optimum tank performance in winter conditions.

1.5 Outline of research

In Chapter 2, the concept of latent energy storages and their design will be reviewed. Also, some current applications of low-temperature PCMs are discussed. A literature review is also conducted on the process of heat loss in storage tanks. Chapter 3 presents a detailed experimental methodology and elaborates the process of formation of the MATLAB model. Subsequently, a sample case is set up in ANSYS Fluent for visualization of the problem. The simulation is simplified in 2D and all assumptions made in the simulation are listed. In Chapter 4, the numerical MATLAB model is validated using the experimental results. Various tank scenarios are then simulated using the validated model to study the impact on tank performance. Finally, the research conclusions and recommendations based on findings are presented in Chapter 5.

1.6 Significance of research and contributions

Climates around close to the earth's north pole, for example in Canada, are generally not suitable for operations of truck engines with B100 biodiesel because of unfavourable cold weather properties. The success of this research can potentially encourage increased use of the fuel for transportation proposes thereby reducing GHG emissions. A higher demand for biodiesel fuel would lead to more investments both by government and private stakeholders in the biofuel industry. Many industrial scale refineries can be built as a result of this investment ultimately leading to a reduced production cost and reduced pricing for the end users. A more competitive pricing for biodiesel is needed to convince some consumers to make the shift from using petroleum diesel.

The contribution of this research is opening a new investigation into alternative ways to improve cold flow behaviour of biodiesel and more creative and beneficial uses of low-temperature phase change materials.

1.7 Crystallization and gel formation in biodiesel

Crystallization is the process whereby a solid phase is formed as a result of atoms or molecules arranging themselves in a highly organized structure known as a crystal. For this to occur, there must be sufficient thermodynamic force generated within the molecules of the solution. This process occurs in many natural phenomena, for example, in the formation of snowflakes. Crystallization occurs in two stages which

are nucleation and crystal growth respectively and both depend on the thermodynamic and chemical properties of the solution. In the nucleation stage, the molecules in the liquid begin to gather into clusters and when they reach a certain critical size they become stable and constitute the solid nuclei or crystal lattice. Subsequently, the crystal growth stage begins whereby the solute atoms or molecules precipitate out of the solution and merge with existing crystal lattices to form larger crystals. The process is determined by the supersaturation of the mixture which depends on the temperature of the solution and its concentration. In a homogeneous mixture, crystallization is determined by the solubility of the constituents [10].

Gelling is a consequence of crystal growth which occurs when the molecules form a continuous network of crystals in a liquid. In biodiesel, at certain low temperatures determined by the saturation of the FAME, crystallization begins and further reduction in temperature accelerates crystal growth and ultimately results in gelling. As will be elaborated in later sections of this chapter, the crystallization point of biodiesel primarily depends on the feedstock used in its production as the level of saturation for various biodiesel feedstock differs widely.

Figure 1.4 shows biodiesel from different feedstocks kept at the same temperature of 35˚F (1.67˚C). It shows that biodiesel made from canola oil still remains clear at that temperature while that made from olive oil has gelled due to crystallization.

Figure 1.4: Different levels of crystallization of biodiesel from various feedstock at the same temperature of 1.67˚C [11].

1.8 Characterization of cold flow behavior of biodiesel

There are five parameters usually used to describe the characteristics of fuel for their use under low temperature conditions. The test procedures have been defined by ASTM International as shown on Table 1.1 and are detailed below.

1.8.1 Cloud point (CP)

Cloud point is the most frequently used parameter for measuring low temperature biodiesel behavior. It is the temperature at which a cloud of wax crystals first become visible when the fuel is cooled under controlled conditions [12]. Cloud point is usually used as a biodiesel quality control check when used in diesel engines at low temperatures, however the parameter itself is not sufficient to predict its cold flow

behavior. This is because, at this temperature crystal formation is only beginning and the biodiesel does not necessarily clog the engine filters. Biodiesel CP varies widely depending on the source of the feedstock, i.e. its fatty acid composition. Atabani et al. [13] presented a list for cloud points and other properties for biodiesel made from a wide variety of non-edible oil seeds. The cloud point of biodiesels in the list ranged from -13.4˚C (castor) to 13.2˚C (polanga). Generally, the CP of biodiesel is much higher than that of petroleum-derived diesel.

1.8.2 Pour point (PP)

The pour point is the lowest temperature at which flow of the oil is observed. When biodiesel attains this temperature, it becomes highly viscous and is no longer able to be pumped. This can be regarded as the advanced stage of crystal growth where the fuel becomes gel-like. The PP parameter is used more as a quality indicator in applications that involve the pipeline distribution or storage of biodiesels. Since fuel filter plugging generally occurs at temperatures much higher than the PP, it is seldom used as a parameter to judge biodiesel usage in CI engines. The PP is always lower than the CP.

1.8.3 Cold filter plugging point (CFPP)

The CFPP can better predict the operability of biodiesel in CI engines because it measures the filterability of the fuel through engine fuel filters in low temperature conditions. It is the lowest temperature at which 20 mL of sample can pass through a 45 μm filter in 60 seconds or less under a controlled vacuum [10]. This is a relatively

more important test to carry out because in cold regions, biodiesel with a high CFPP will clog up engines easily.

1.8.4 Low temperature filterability test (LTFT)

The LTFT gives the temperature at which 180 mL of a sample can pass through a 17 μm filter in 60 seconds or less. The test sample is cooled at interval of 1˚C until the minimum test criteria is met. Both the CFPP and LTFT are similar, however, since the LTFT better reflects the rigorous conditions experienced in diesel engines, it is considered as a better approach [10]. The CFPP and LTFT have been shown to be linearly proportional to CP [14].

1.8.5 Cold soak filtration test (CSFT)

Under specific conditions, some biodiesel tend to begin crystal formation above cloud point and these crystals do not re-dissolve after returning the biodiesel to a higher temperature. The cold soak filterability is the newest requirement which was added in 2008 to address this issue. It involves cooling 300 mL of biodiesel for 16 hours, removing the sample from the chiller and then letting it return to room temperature. The sample is then filtered through a 0.7 μm filter paper and the time recorded. The maximum allowable time for this test is 360 seconds [15]. Cold soak filtration is now used along with cloud point, especially in blends to predict the low temperature operability of biodiesel.

The determination of the best indicating parameter to use depends on the application of the biodiesel. However, for the purpose of this research, the CP is used as an indicator of cold weather operability. Since crystals begin to form at this temperature,

negative impact on engine filters and fuel lines are likely to begin at this point. Table 1.1 shows the standard test methods used for the five parameters discussed in this section.

Table 1.1: ASTM International standards for biodiesel cold flow characterization

Parameters	Standard test methods
Cloud point	ASTM D-2500
Pour point	ASTM D-97
Cold filter plugging point	ASTM D-6371
Low temperature filterability test	ASTM D-4539
Cold soak filterability	ASTM D-7501

1.9 Improving the cold flow behaviour of biodiesel

Research work has been performed and is still being conducted to make biodiesel suitable for winter applications. Some of the methods proposed by researchers have been successful in improving cold flow properties of biodiesel; however, there is a resulting undesirable trade-off on the ignition quality and oxidation stability of the fuel. This is because the saturated portion of the biodiesel, which is responsible for the poor cold behavior of biodiesel, has a positive impact on its ignition quality and oxidation stability [10]. Furthermore, most of these methods increase the overall production cost and makes biodiesel less attractive to the end users. The following methods are currently utilized to improve the cold flow performance of biodiesel.

1.9.1 Blending with petroleum derived diesel

Biodiesel is most commonly used as a blend with petroleum diesel [9]. Since the cold flow properties primarily depend on the fatty acid profile of the fuel, mixing biodiesel which has a high saturation of fatty acids with oil which is high in unsaturated fatty acids (typically petroleum diesel) will result in a blend with enhanced cold flow properties [16]. This principle also applies to blending biodiesel with oil with short chain or branched chain hydrocarbon. A number following the letter "B" specifies the percentage of biodiesel by volume in a fuel sample – for example, pure biodiesel is referred to as B100. ASTM D975 specifies the use of up to 5% vol. concentration (B5) in biodiesel blends to serve the same application as pure petroleum diesel without the need of any engine modifications. Previous research has shown that a 20% by volume biodiesel in diesel fuel #1 and a 35% by volume in diesel fuel #2 is required to produce the best results [17].

1.9.2 Transesterification with a branched or higher molecular weight alcohol

Transesterification of fatty acids can also be achieved with other alcohols than the commonly used methanol. The use of branched chain alcohols result in a more branched fatty ester structure and this reduces the crystallization temperature and cloud point [10]. Bejan et al. [18] investigated the effect of using methyl, ethyl, isopropyl and benzyl alcohol to produce biodiesel using palm feedstocks. The results showed that the use of isopropyl alcohol gave a biodiesel with the lowest CFPP of -16˚C while the use of benzyl alcohol yielded a biodiesel with high viscosity which

failed to meet the international specifications. The increase in viscosity observed could be as a result of the higher molecular weight of the alcohol.

One disadvantage of using branched or higher molecular weight alcohol is that they are more expensive and would result in increased production cost. Some researchers have also reported that the use of branched alcohols have resulted in worsened ignition quality [19], and oxidation stability [20].

1.9.3 Use of chemical additives

Fuel additives are commonly used to improve the properties of petroleum products to provide better engine performance. Depending on the type, additives can be useful to improve cetane number, lubricity, combustion and cold flow properties amongst others. As is common in petroleum products, additives can also be used with biodiesel in a similar manner to improve its cold flow properties. They are also regarded as cold flow improvers (CFI). Biodiesel additives are usually polymeric (e.g. polyacrylate or polymethacrylate) or metallic (e.g. magnesium, nickel, manganese) derivatives that improve cold flow behaviour by preventing crystal formation, impeding its organization which would result in agglomeration, or altering the crystal from an orthorhombic to a needle-like shape for easy passage through engine filter to prevent the plugging of engine fuel lines [10], [21]. There several types of additives including CFPP depressants, PP depressants and wax crystalline modifiers. Work by Chastek [22] studying over 13 polymers showed that poly (lauryl methacrylate) improves the cold flow properties of biodiesel most effectively. The research indicated that at a concentration of 1%, the pour point of the biodiesel was lowered by as much as 30˚C.

Chiu et al. [23] also studied the effect of cold flow improvers on soybean B100 and B80-B90 biodiesel blends using different additives in the concentration of 0.1-2%. The work showed that a mixture of 0.2% Bio flow-875® additive, 79.8% biodiesel and 20% kerosene reduced the PP of B100 soybean biodiesel by 27˚C.

While the use of certain additives has recorded success for improving the cold flow properties of biodiesel derived from specific feedstocks, no single additive has recorded significant improvement in cold flow properties across a wide variety of biodiesel from different feedstocks. Therefore, the additive used should be suitable for each kind of biodiesel in order to meet all biodiesel specifications [16]. Certain researchers have also reported insignificant cloud point reduction and lower flash point when using additives on biodiesel [10].

1.9.4 Cold fractionation

This process is also referred to as winterization and has been generally used in the past to improve the quality of fats and oils. Cold fractionation involves cooling the oil to a low temperature between its cloud point and pour point and allowing the saturated fatty acid components to precipitate out of the oil after which it is separated. This process is repeated in several stages, successively lowering the saturated fatty content of the biodiesel until no more crystals are forms after the oil sample is held at the temperature for more than three hours [10]. However, a major disadvantage is the high yield losses associated with fractionation. Cold fractionation process carried out on waste cooking biodiesel by cooling 0.2˚C below PP in a three-stage winterization process led to an overall loss of 12.6% and cloud point lowered

from 14.5˚C to 9˚C [24]. Another research recorded that winterization on palm biodiesel produced losses of 57.7% while the CP was lowered to -9˚C [25]. Generally, the process is relatively expensive due to the number of stages required and the high losses associated. Also, the resulting biodiesel has lower ignition qualities due to the decreased saturated fatty acid content. Table 1.2 summarizes the challenges of using the various methods of improving cold flow behaviour of biodiesel as discussed above.

Table 1.2: Reported challenges for using various methods of improving cold flow properties of biodiesel

Method	Reported challenges
Blending with petroleum diesel	• High production cost due to additional stage of blending
Transesterification with branched chain or higher molecular weight alcohol	• High production cost • Reduction in cetane number • Transesterification reaction rate lowers with increasing alcohol molecular weight • Lower yields and incomplete transesterification reaction • Higher biodiesel viscosity
Use of chemical additives	• Insignificant cloud point reduction • Lower flash point • Choice specific to biodiesel feedstock
Cold fractionation	• High losses resulting in low yield • Lowered cetane number • High production cost due to more energy and time consumption

1.10 Hypothesis: using phase change materials (PCM) as an alternative approach in a biodiesel tank design can extend the time before clouding begins

Using these methods just discussed above, the CP of some biodiesels have been reduced significantly, but as highlighted no single method have been successfully applied without a trade-off on some desirable fuel property. Moreover, in very cold regions like Canada, which experience extremely low temperatures of up to -30˚C in winter, the methods outlined above may not be very effective. Hence, biodiesel is most commonly largely blended with petroleum diesel to prevent clouding or gelling. Most engine manufacturers even limit the amount of biodiesel in the blend to 5% (B5) in winter for warrantee purposes [27].

To overcome the challenges of the higher cloud point of biodiesel in colder regions, electric heaters and coolant fuel warmers have been frequently implemented in vehicles and biodiesel storage tanks. While solely relying on an electric biodiesel tank heater solves the problem, it can be energy intensive. Furthermore, using just coolant fuel warmers is not so effective when the engine is not in operation and left out in extreme winter temperatures for several days without an electric heater backup. The high thermal heat losses associated with these applications can be reduced by insulating the fuel tank; however, to further extend the period in which the biodiesel temperature stays above the CP or CFPP, the present research proposes to investigate implementing a phase change material (PCM) in the tank design.

PCMs absorb or release latent energy during phase change while maintaining a relatively constant temperature. In this application, the PCM of interest are those which undergo solid-liquid transformation. Over the years, they have found many applications in areas like industrial heat recovery, building design, air conditioning, electronic devices, textile design, healthcare and logistics [28]. For example, Rentas et al. [29] designed a container implementing both vacuum insulated panels and phase change materials to store red blood cells (RBC). With this design, it took about 97.4 hours for the temperature of the RBC to fall from 5 to 1˚C. This was a 316% increase in the time period for the design without the PCM. In all the applications, the most important selection criteria for a PCM is the phase change temperature. A reference list has been provided in literature with about 250 PCMs with a very wide phase change temperature range [30].

Modern automobile engines convert approximately 30% to 40% of heat from fuel combustion into mechanical work [31], while the heat remaining is discharged to the surroundings through the exhaust and radiators. In cold regions, part of the waste heat produced from combustion is used to heat up the cabin of the vehicle for passenger comfort. Most of this heat wasted to the environment can be captured and stored in PCMs for use in keeping the temperature of the biodiesel in the tank above CP or CFPP for extended periods of time when the truck is not operating. The concept of waste heat storage in PCMs have been reported by several authors like Kauranen et al. [32], being used for the application of cold-start optimization of engines. Also,

Gumus [33] designed a system using PCM for the preheating of internal combustion engines in cold regions to reduce cold-start emissions.

The process of heat loss in tanks is a transient phenomenon and involves various modes of heat transfer. Within the fluid contained in the tank, the heat transfer is predominantly by conduction and natural convection. Natural convection dominates at the initial stage of cooling, but with time the fluids become more viscous and inhibits convection leading to conduction dominating the heat loss process. Several authors have reported both experimental and numerical analysis of transient heat loss of fluids contained in tanks; however, the heat loss process of tanks containing latent energy storage systems remains mostly undocumented.

Figure 1.5 shows a tractor trailer which could operate potentially on B100 in winter condition where the exiting fuel tanks would be modified to include PCM and a glycol heater.

Figure 1.5: Diesel tractor-trailer truck to operate with B100 in winter. The goal is to retrofit the existing fuel tanks with a PCM heated system so that there is limited change to the configuration and operation of the truck. Image source: [26].

1.11 Is biofuel and PCM as a viable solution on par or better than other alternatives?

1.11.1 Comparison of electric heating with latent energy storage systems in fuel tanks

In certain regions, the cost of electricity is relatively cheap. A good example is in Manitoba, Canada where the cost of electricity in 2017 was 7.381¢/kWh. As a case study, consider a case where energy is stored in a phase change material (PCM) with phase change temperature of 18°C. If the useful energy capacity of the PCM is 250 kJ/kg and we are to make use of 14 kg of the product to preserve the temperature of the biodiesel above cloud point, then the total energy stored is 3,500 kJ or 0.972 kWh. Going by the cost of electricity it would cost ¢7.174 to use an electric heater to transfer the same amount of energy to the biodiesel. This is the equivalent of using a 500 W heater for 1.94 hours. In countries with relatively more expensive electricity, like Denmark and Germany with 0.308 and 0.298 euros (37 and 36 cents) per kWh respectively, as at 2016 [34], the overall cost of heating the biodiesel still would not be very significant.

This analysis brings about the question of the advantage of using PCMs over electric heating. First, this technology proves useful for trucks travelling long distances in the winter, especially to remote locations where electricity may not be readily available for heating. Since the PCM stores waste heat from the engine, this heat can be used to compensate for the heat loss from the biodiesel for several days until electricity is available for heating. In this scenario, the use of PCM in the fuel tanks does not serve to totally replace electric heating, but to serve as backup and also

reduce the number of times the driver would have to stop over to heat the biodiesel which would result in downtime.

The second advantage of using PCMs in fuel tanks is due to relatively lower heat losses to the environment. This is due to the phenomenon of latent heat storage at a lower temperature. As with the previous case discussed, assume that a B100 biodiesel sample of 100 kg (113 liters) is heated with the same amount of energy, 3,500 kJ. If we assume as is typical, that the specific heat capacity of the biodiesel is 2,000 J/kgK and its initial temperature is 5˚C, this would result in a final temperature of 22.5˚C. If the volume of the biodiesel sample is lower, the final temperature even increases further, thereby increasing the temperature difference between the biodiesel and ambient and the heat losses. However, using PCM in the fuel tanks stores significant energy at a lower temperature depending on the phase change temperature of the product used.

1.11.2 Comparison of electric vehicles (EV) to using B100 biodiesel in winter

In the recent years, electric vehicles have begun to gain popularity in Asia, Europe and the Americas due to the increasing concern about climate change. Norway, the global leader in EVs, for example, plans to phase out conventional gasoline and diesel engine and end their sale by the year 2025 [35]. China and other Asian countries like India have also taken similar steps in a move to curtail the menace of rising concentration of greenhouse gases. Despite the successes EV technology has recorded, they are still a long way from being implemented on heavy-duty trucks. The biggest challenge in making EV heavy-duty trucks viable is the current battery technology.

Due to the amount of power that will be required to drive trucks, an EV truck with current battery technology will have reduced load capacity for commercial vehicles. Consequently, in October 2017, the Volkswagen Group made a commitment of $1.7 billion to researching on making EV more attractive to trucking and delivery companies by 2020 [36]. Before EV trucks can be practical, more research has to be done on making batteries much more efficient so their sizes can be reduced.

Other problems that an EV truck would face, just like the current electric cars, are limitations in range and high initial cost. Intermittent charging can also create significant downtime for trucking and delivery companies. In contrast, B100 biodiesel may be used in current heavy-duty diesel trucks with little modifications to the fuel storage systems to enable its cold weather operability; which is part of the objectives of this research. In the end, there is a market place for both renewable energy options.

1.12 Research methodology

The design described in this research have been made specifically for experimental purposes. The actual biodiesel fuel tank to be implemented in engines will be a modification to the already existing fuel tank. However, the essential components and concepts presented here are all applicable in the actual design. The design as shown in Figure 1.6 consists of a tank shell made of aluminum which contains the biodiesel fuel. Various removable aluminum alloy tubes filled with a PCM with desired phase change temperature are then introduced through the top of the tank.

The PCM tubes do not contact the base of the tank to prevent additional heat loss by conduction. A biodiesel fuel warmer is introduced at the top of the tank to heat up the fuel using hot fluid. In compression-ignition engines, the hot fluid will be provided by the ethylene glycol engine coolant. This fuel warmer is a heat exchanger made from stainless steel tubing. Copper tubing, despite their high conductivity, was not used because of the compatibility challenges with B100 biodiesel due to the risk of accelerated oxidation [37]. The aluminum tank shell is insulated using extruded polystyrene insulation (not shown in the diagram). To make the design more compact, future design could consider using vacuum insulated panel which would come at an extra cost. For the experiment canola oil is used in place of biodiesel due to safety regulations at the University of Manitoba on using large amount of flammable fuels. However, the thermal behaviour of canola oil and biodiesel are both similar, since both exhibits Newtonian properties at temperatures above cloud point. Therefore, a proof of concept using canola oil will be directly applicable to B100 biodiesel.

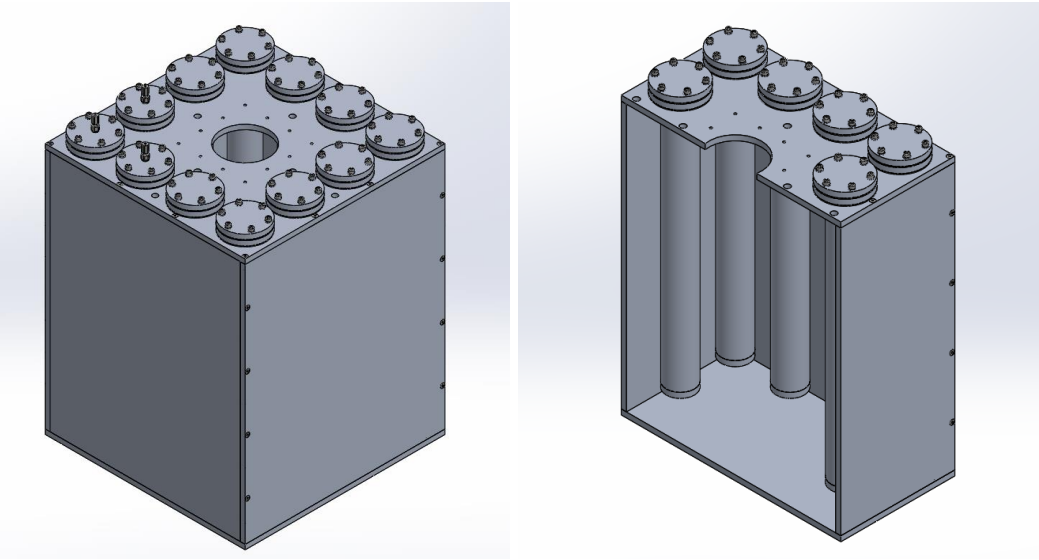

Figure 1.6: Biodiesel tank model assembly (left), and sectional tank view (right)

The tank design could be implemented into an existing truck using a bypass connection to the radiator of the engine, as shown in Figure 1.7. The biodiesel tank would contain a temperature sensor which provides feedback to a valve actuator to switch on and off. The charging cycle occurs when the engine is in normal operation and the average temperature of the biodiesel in the tank is below a setpoint temperature, a signal is sent to the valve to open. A portion of the ethylene glycol coolant would then pass through the biodiesel tank loop to heat up the fuel. In the process of heating up the fuel, heat is transferred from the biodiesel to charge up the PCM by storing latent energy at a relatively low temperature.

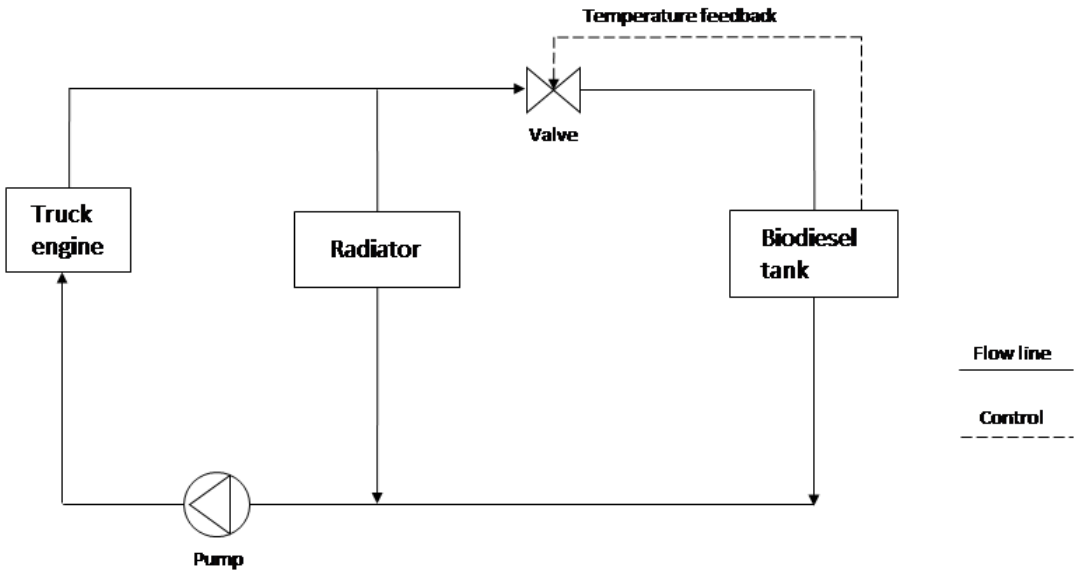

Figure 1.7: Schematic of implementation of tank design to heavy duty trucks

Figure 1.8 shows a schematic of how a commercial B100 truck tank would potentially be designed according to the hypothesis of using PCM. Holes can be made at the top of existing tanks with other slight modifications to use PCM in the design.

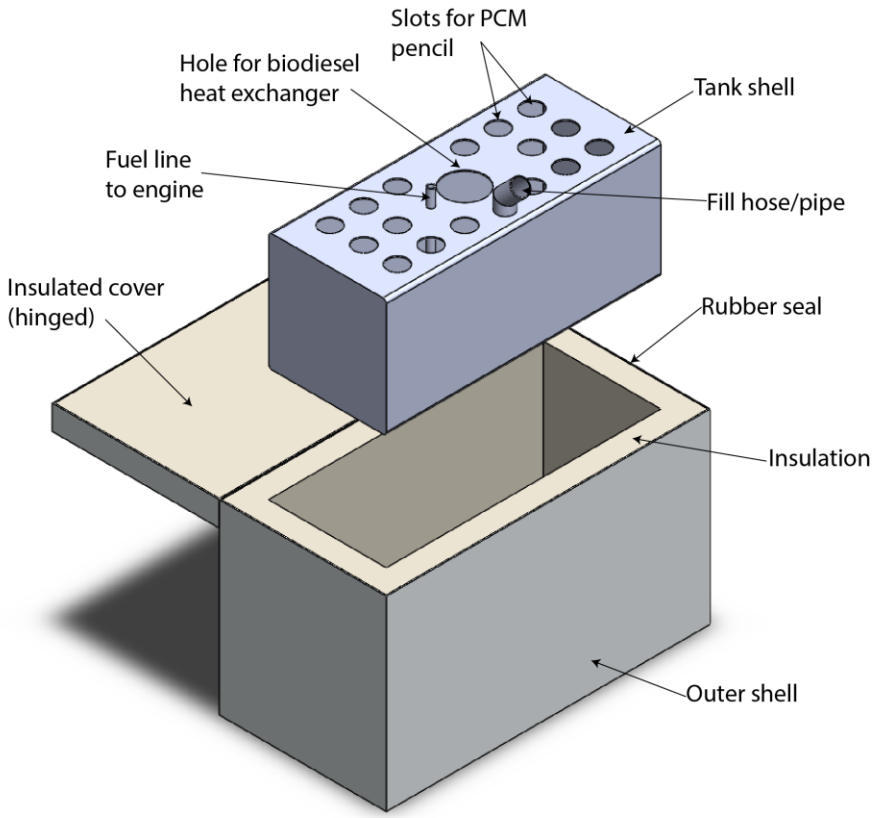

Figure 1.8: Schematic of a sample 100 litre biodiesel fuel tank with

The procedure to carry out this research involves first performing an experimental using the proposed tank design by subjecting it to temperatures as low as -20°C in the wind icing tunnel at the Thermofluids Engineering Laboratory of the University of Manitoba. Subsequently, a simplified MATLAB model is developed for the problem which is validated by the experimental results. ANSYS Fluent 17.2 is then used for visualization study in a sample scenario. Based on the experimental and numerical results, recommendations are then made for an optimum biodiesel tank design for implementation in an existing diesel truck engine.

2

Phase change materials and heat loss in tanks

2.1 Energy efficiency and waste heat utilization

Energy efficiency and sustainability has been the motivation for many researches going on in various engineering fields today. In many engineering processes, wasted energy is usually obtainable in the form of heat. A classic example is the Rankine cycle where mechanical energy is generated from a turbine in a process which cannot be sustained without the presence of a condenser which discharges heat from the working fluid thereby transforming the wet vapour into a saturated liquid. This heat loss stage is an inevitable requirement to drive the cycle and determines the efficiency of the Rankine cycle. The heat is usually discharged through cooling towers or a large body of water like the river or sea. A similar analogy could be made for engines or equipment that generate excess heat from their operation and which will have to be discharged to prevent overheating that can ultimately damage the systems.

From the second law of thermodynamics, we can infer that it is impossible to eliminate waste thermal energy from a system, however it is possible to capture this energy and store it for use in other processes which would require additional sources of energy. The captured thermal energy could also be redirected to the parent system to improve its overall efficiency. Various technologies which currently exist for the recovery of process waste heat include heat exchangers, steam Rankine cycles, organic Rankine cycle, absorption chillers, mechanical vapour compressors (MVC) and absorption heat pumps [38]. A detailed classification of the existing technologies is presented in Figure 2.1. Despite its useful potential, industrial waste heat utilization is still not widely adopted today because of the inability of the utility to use it all at the time of availability and the inexpensive cost of using fossil fuels to generate thermal energy [39].

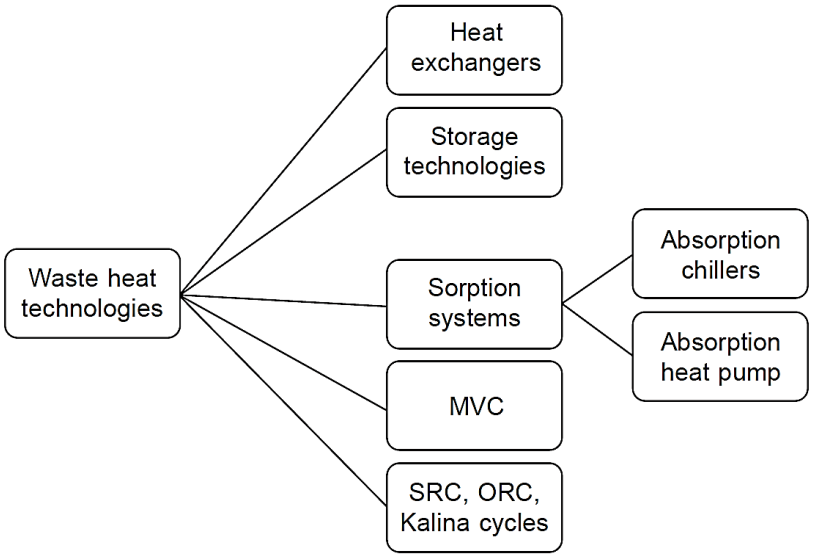

Figure 2.1: Technologies for process waste heat recovery. MVC – Mechanical Vapour compressors; SRC – Steam Rankine Cycle; ORC – Organic Rankine Cycle [40].

2.2 Thermal energy storages (TES)

Thermal energy storages (TES) are systems designed for storage of heat or cold depending on the application. As highlighted in the previous section, TES can improve the overall efficiency and reliability of utilities by serving as a reservoir to compensate for mismatches between energy demand and supply [41]. Thermal energy can be stored in materials in various forms which include thermochemical, sensible and latent energy.

Thermochemical energy storage in material is based on the use of the heat of reaction in a reversible chemical reaction [42]. As an example, when Calcium carbonate is heated, it decomposes to calcium oxide and carbon dioxide, absorbing the reaction energy. This stored energy is then released when the temperature of the system falls below a threshold temperature reversing the reaction. Calcium carbonate and similar materials like Calcium hydroxide and Manganese oxide are also being currently researched for concentrated solar power plant applications. However, most current technologies are still at laboratory scale [43].

In sensible energy storage, thermal energy is stored in a material through the rise of its molecule's vibrational energy leading to a rise in the its temperature. The amount of energy stored in a material is given by Equation (2.1).

$$Q = \int_{T_1}^{T_2} mC_p \, dT = mC_p(T_2 - T_1) \tag{2.1}$$

Where m is the mass of the material, C_p is its specific heat capacity and T_1 and T_2 are the initial and final temperatures as a result of energy addition or extraction. The specific heat capacity is a property of the material that designates the amount of energy needed to raise the temperature of one kilogram of the material by one Kelvin. Sensible TES has found a wide variety of application by using common materials like water, concrete or stones. Water as an example is employed in many domestic hot water and CSP applications. A notable commercial application of water is the heat storage pit in Vojens which has a capacity of 200,000 m^3 to store thermal energy generated from 70,000 m^2 of solar collection area. The district heating installation has an annual energy generation of 28,000 MWh and meets about 50% of Vojens' total heating demand [44]. Despite the ease of application of sensible energy storage technologies, some of its disadvantages are that energy cannot be stored or extracted at constant temperature, and it requires a large amount of storage medium to store significant energy in comparison to the other TES methods.

Latent energy storage is achieved by the process of phase change in materials which happens as a result of a reorganization of its molecular structure. The latent energy is stored or released during the change of state which could be from solid to solid, liquid to gas, solid to gas or solid to liquid. However, the most popular phase change process used is the solid to liquid transformation due it relatively simple application and lower volume change [39]. The amount of energy stored in a material which undergoes a complete phase change can be calculated using Equation (2.2).

$$Q = \int_{T_1}^{T_m} mC_p \, dT + mL + \int_{T_m}^{T_2} mC_p \, dT \tag{2.2}$$

Where L represents the latent energy in kJ/kg which is a property of the material.

In contrast to sensible heat storage, an advantage of latent energy storage is that energy can be stored and retrieved at a relatively constant temperature and that some specific materials have high latent energy storage capacities which reduces the amount of material required to store the same amount of energy. Figure 2.2 shows a comparison of the theoretical latent heat curve to that of sensible heat.

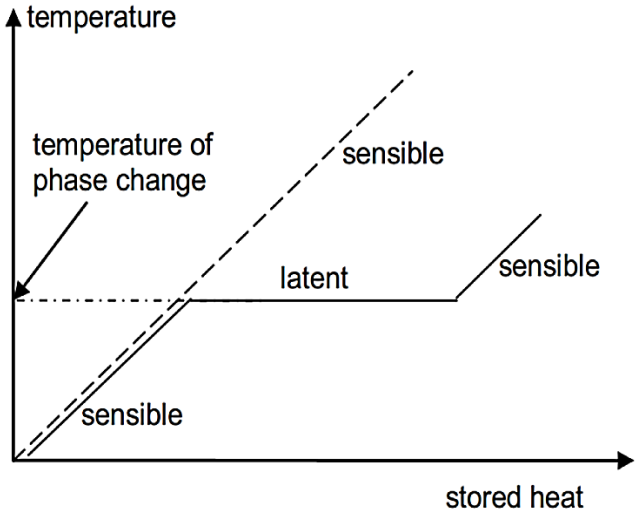

Figure 2.2: Comparison of theoretical latent heat curve for a phase change process to sensible heat [41].

2.3 Phase change materials (PCMs)

Materials that absorb or release a relatively large amount of energy during their phase change transformation are known as phase change materials (PCMs). In

addition to a high storage density, they also have several advantages including low temperature fluctuation during storage or extraction and temperature flexibility due to the wide variety of PCMs available commercially at different phase change temperatures depending on the application. To be chosen as a suitable PCM, a material should exhibit a good combination of attributes such as repeatable phase change, high thermal conductivity, small volume change, congruent melting, minimal supercooling, chemical stability, material compatibility, affordability, amongst others [41]. Practically, no single material can meet all the requirements, therefore, occasionally compromises can be made and the shortcomings can be accommodated for by using an improvised storage system design [30].

PCMs that transform from solid to liquid during the phase change process will be specifically considered in this research due to the reasons highlighted in the previous section. They are broadly classified into organic, inorganic and eutectic PCMs.

Organic PCMs consist of paraffins and non-paraffins (fatty acids). Paraffins are a group of long-chain saturated hydrocarbons of the form C_nH_{2n+2} with high latent heat of fusion (60 -269 kJ/kg) [45]. Generally, the longer chain hydrocarbons possess higher melting point and latent heat of fusion. They are generally the most commercially used PCM group due to reasons such as chemical stability, reliability, good heat of fusion, and affordability. Other favourable attributes and shortcomings of organic PCMs are highlighted in Table 2.1. Its major disadvantage is its low thermal conductivity (i.e. range of 0.2 W/mK), but this shortcoming can be addressed by implementing a fin design in the storage unit for better contact area or the use of

highly conductive thermal additives such as carbon fibres or metal based materials [46]. Yin et al. [47] improved the thermal conductivity of a PCM from 0.27 W/mK to 0.46 W/mK by preparing a composite made by absorbing liquid paraffin into the pores contained in expanded graphite. Non-paraffins essentially consists of fatty acids of type $CH_3(CH_2)_{2n}COOH$ which have high latent heat of fusion (125-250 kJ/kg) and other properties similar to paraffins, but they are 2 to 3 times more expensive than the latter.

Inorganic PCMs are further categorized into salt hydrates and metallic alloys. Salt hydrates which are of type $AB \cdot nH_20$ have much higher latent heat per unit volume, higher thermal conductivity (i.e. range of 0.7 W/mK), good price and are currently the most studied groups of PCMs. Their melting and solidification are as a result of the dehydration and hydration of the salt. Generally, the typical melting temperatures of most salt hydrates range from -33℃ to 120℃ and heat of fusion from 86-326 kJ/kg [30], [45]. Their major disadvantage, however, is their corrosive nature which leads to higher maintenance cost in the long term. Cabeza et al. [48] conducted an investigation into the short-term compatibility of aluminium, brass, copper, steel and stainless steel by immersing them in different salt hydrates including zinc nitrate hexahydrate, sodium hydrogen phosphate dodecahydrate and calcium chloride hexahydrate for a period of 3 days, 1 week and 2 weeks. Their results indicated that zinc nitrate hexahydrate was extremely corrosive to all other metals tested apart from stainless steel. They also found that calcium chloride hexahydrate was compatible with brass and copper, while corrosive against the other metals tested. In

addition, it was observed that sodium hydrogen phosphate was compatible with brass, copper and stainless steel, but corrosive against aluminium. These behaviours indicate that special care must be taken in the design of storages of which inorganic salt hydrates are to be used. Another problem with salt hydrates is that they exhibit incongruent melting which occurs when the salt is not entirely soluble in its water of hydration. The insoluble salt then sinks to the bottom because its density is higher than water. Unfortunately, incongruent melting is an irreversible process and it reduces the storage efficiency of the design. Metallic alloys on the other hand, despite their high conductivities, are currently not widely studied because of their larger weight which limits their application.

Eutectic PCMs also show great potential for commercial application. They consist of a combination of inorganic-inorganic, inorganic-organic, or organic-organic PCMs. A major advantage is that each of the constituent of the composition melts and freezes congruently without segregation, which enhances the heat transfer process. Despite their good thermal conductivity and high heat of fusion, their major drawback is their high cost. Table 2.1 summarizes the advantages and disadvantages of the various categories of PCM just discussed. From the comparison based on their melting points, thermal conductivities, latent heat, cost, amongst others it has been reported that paraffins and salt hydrates currently provide better thermal energy medium than the others [45].

Table 2.1: Advantages and disadvantages for various categories of PCM [45]

Category	Sub-category	Advantages	Disadvantages
Organic	Paraffins	• Chemically stable, non-corrosive • High latent heat of fusion • Commercially available at good price • Minimal supercooling or segregation	• Low thermal conductivity • High volumetric change • Poor compatibility with plastic containers • High flammability
	Non-paraffins (fatty acids)	• High latent heat of fusion • No supercooling • Sharp phase transformation	• Low thermal conductivity • Chemical instability at high temperatures • More expensive than paraffins • Toxic and corrosive
Inorganic	Salt hydrates	• High thermal conductivity • Low volume change • High latent heat of fusion • Commercially available at good price • Sharp phase transformation	• Tendency for phase segregation • Higher supercooling • Corrosive and slightly toxic • Poor thermal stability
	Metallic	• High thermal conductivity • Low vapour pressure	• Low specific heat capacity • High cost • Low heat of fusion • Very high weight (density)
Eutectics		• Good thermal conductivity • No phase segregation	• Low heat of fusion • Expensive

2.4 Design of latent energy storages

Due to the low thermal conductivity of PCMs, material compatibility and thermo-physical stability issues, special consideration should be given to the design to enhance the shortcomings of the storage system. The PCM is usually selected based on the phase change temperature needed for the application in addition to other criteria discussed in the previous section. After PCM has been selected, the design of the PCM storage and its implementation plays an important role in the system's overall performance. Latent energy storages can be broadly categorized into active and passive systems [41]. In an active system, the heat transfer fluid (HTF) is being actively moved through some means of forced convection such as a pump or fan to transfer energy to and from the PCM, while in a passive system, the method of heat transfer to and from the PCM is by free convection or pure conduction. The decision on whether to use an active or passive system for an application and primarily depends on how thermal energy can be conveniently transferred from the heat source and stored in the PCM. However, it is important that the system is as simple as possible to reduce the overall thermal resistance of heat transfer and storage.

The most common types of active latent energy storages are those designed in form of heat exchangers to exchange heat between the PCM and HTF. Figure 2.3 shows an illustration of this storage type. Figure 2.3(left) shows the first type, where the HTF flows around a set of PCM modules contained in heat exchanger. Different form of design geometries currently exists for this kind of storage such as tubular, rectangular, dimple sheets or spherical capsules. The method of heat storage in these

geometries is known as 'macroencapsulation'. The method has gained popularity in solar thermal applications like for domestic hot water and space heating purposes. Kaygusuz [49] conducted an experimental and theoretical investigation to determine the performance of calcium chloride hexahydrate PCMs for solar water-heating systems. The system consisted of a solar collector, energy storage tank, and other equipment used to transfer heat collected from the solar array for storage in 1,500 kg of PCM contained in horizontally positioned cylindrical tubes installed in the tank. The HTF was water, which flowed parallel to the PCM containers to transfer the thermal energy. The result obtained indicated that the PCM could be used as a better heat source alternative to rock and water storage systems especially in a solar-assisted heat pump for domestic heating.

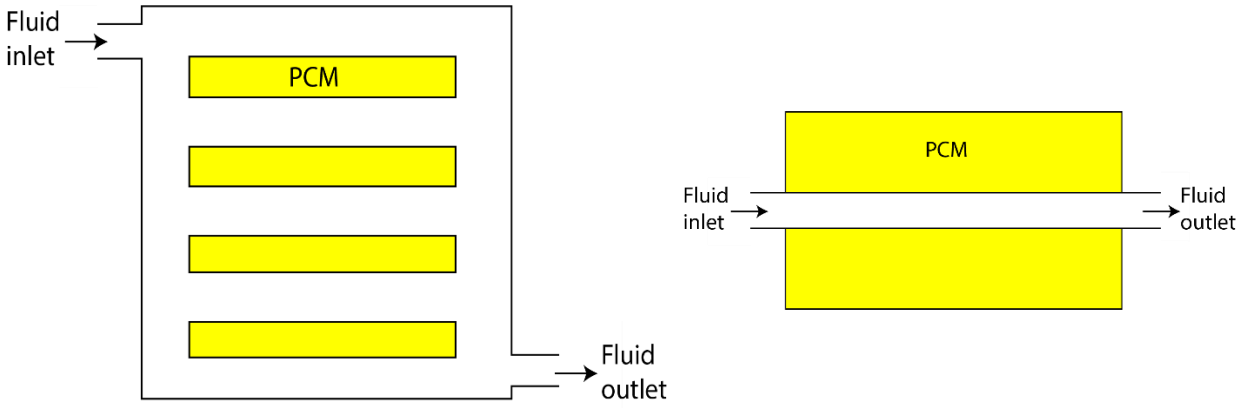

Figure 2.3: Active latent energy storage systems. Shell-tube heat exchanger style (left), and tube-in-tank style (right).

Gumus [33] also designed a thermal energy storage device (TESD) using sodium sulphate decahydrate PCM for preheating internal combustion engines in cold regions to reduce cold-start emissions. The TESD was connected to the water jacket

of the engine to capture waste heat from the engine radiator with the aid of an electrical pump. It was observed that the temperature of the engine increased by 17.4℃ by preheating of the engine and the CO and HC emissions were reduced by 64% and 15% respectively at an ambient temperature of 2℃. The second type of active latent energy storage is shown in Figure 1.3(right) where the HTF fluid flows through a tube or duct enclosed by a layer of PCM to store the heat or cold. Due to the low thermal conductivity, the largest resistance to heat flow is on the PCM side. Extended surfaces such as fins can be implemented into the design or graphite and other metallic structures added to the PCM to improve the efficiency of heat storage and extraction. Ibrahim et al. [50] published a review paper on various state-of-the-art heat transfer enhancements of PCM for TES applications.

Less common types of active latent thermal storages are the slurry type where the microencapsulated PCM is immersed in the HTF and they can both be stored in a tank together or pumped out as a single mixed fluid, and the direct contact storage where the HTF flows through a non-encapsulated bed of PCM which is immiscible with the fluid, eliminating the additional thermal resistance of the heat transfer wall [41].

Passive latent energy storages as earlier highlighted depends primarily on natural convection or pure conduction for the transfer of stored thermal energy. They typically have lower capacity due to the low thermal conductivity of PCMs and relatively lower heat transfer coefficient especially when the heat is being transferred to a gas [41]. As a result, they find a wider application in areas where the PCM is

used for temperature control purposes. The amount of PCM used in these applications then depends on the time during which the temperature control is required. Figure 2.4 presents a schematic for the implementation of passive latent energy storages. In the first type shown in Figure 2.4(left), the PCM storage and demand which are in the same container exist as two separate units. This is usually the case when the demand is an entity such as temperature sensitive goods, the human body or electronic equipment. The heat is transferred from the PCM to the body either by direct contact (conduction) or indirectly by natural convection through the ambient fluid. The whole system (demand) usually also insulated to reduce overall heat loss to the environment. A typical example is the use of ice packs to cool beverages or the use of macroencapsulated PCM to preserve the temperature of red blood cells which was applied by Rentas [29] as earlier described in Chapter 1. This method is also gaining popularity in the design of building components like floors, walls and roofs for passive application.

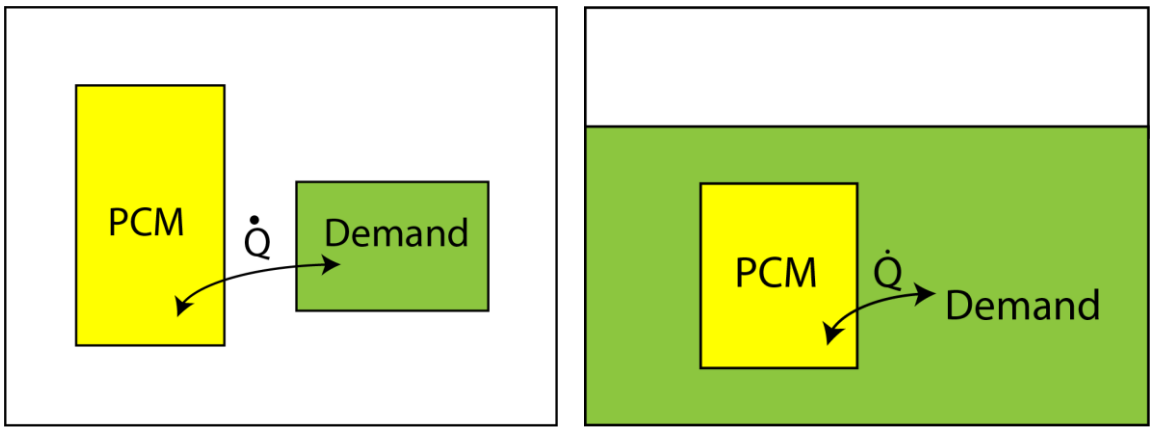

Figure 2.4: Passive latent energy storages. Storage and demand as separate units (left), and storage immersed in demand (right).

Shilei et al. [51] investigated the impact of a phase change wall room on indoor thermal environment during winter in northeast China. They constructed a phase change wall board from gypsum board and PCM and attached to the surface on an ordinary room. The temperature fluctuations were then compared to the room without the PCM boards and the results indicated that the PCM wallboard significantly reduced temperature fluctuations in the room, thereby improving comfort and helping to energy costs from heating. In the second type of passive latent energy storage shown in Figure 2.4(right), the PCM storage is immersed either completely or partially in the demand which is usually a liquid. Heat transfer from the PCM to the liquid in this case would be by natural convection. Passive latent thermal storage has also been applied in solar thermal energy water storage systems to preserve the temperature of water during night time when there is no energy generation for morning use. The experimental investigation conducted Canbazoğlu et al. [52] into the use of sodium thiosulphate pentahydrate PCM to improve the performance of a solar thermal energy storage indicated that the temperature at the midpoint of the storage tank remained at a constant value 45℃ for a period of almost 10 hours during the night time until the sun rose again for more energy generation. It was further observed that the overall mass of produced hot water was 2.59 to 3.45 times that of a conventional solar water-heating system without the PCM installed.

2.5 Heat transfer analysis and modelling of latent energy storages

The literature survey in the previous section has shown that the phase change temperature is one of the most important selection criteria for PCMs. An appropriate selection ensures repeated melting and solidification cycles [41]. It is also relevant to understand the heat transfer processes involved in PCM to adequately design thermal energy storages or predict the performance of the systems.

The phenomena of melting and solidification is widely studied and applies in a wide range of industrial processes like solidification of castings and metal processing. In these phenomena, there exists a moving boundary that separates the solid and liquid phases which have unique transport and thermal properties in which the instantaneous position of the moving boundary is unknown a priori, but must be determined as part of the solution.

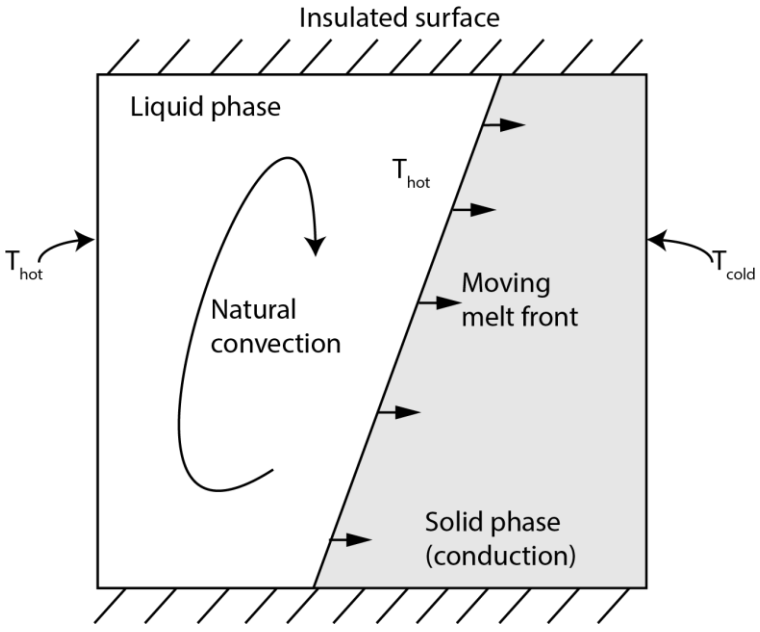

Figure 2.5: Schematic illustration of 1-D melting in a rectangular enclosure

Figure 2.5 shows a one-dimensional illustration of a moving boundary for a melting and solidification within rectangular enclosure. It is observed that the melting front which is at the phase change temperature becomes skewed as the natural convection effect in the liquid phase becomes more dominant [53]. The strength of the natural convection depends on the dimensions of the enclosure and is suppressed in many applications in which the effect could be ignored during modelling without significant impact on the accuracy of the prediction [54].

In the early days, the Stefan problem was an analytical model used to study melting and solidification process, but applied mostly to one-dimensional semi-infinite regions with simplistic assumptions of thermophysical properties and boundary conditions [55]. However, this model is not practical as many real phase change scenarios are rarely one dimensional with complex boundary conditions and thermophysical properties. Neumann further developed Stefan's problem to the two-phase problem with more realistic assumptions and boundary conditions, but its solution was only applicable to moving boundary problems in the rectangular coordinate system [56].

2.5.1 Numerical modelling of PCMs

With advancement in numerical methods over the years, several methods are now popularly being used to model melting and solidification in PCMs. These models predict the phase change problems more accurately and realistically, and can be applied to a wider range of complex geometries as opposed to the Stefan and

Neumann models. The most commonly used methods are the enthalpy method and enthalpy-porosity approach.

In the enthalpy method, the time evolution of the energy contained in the PCM is accounted for by the relationship between enthalpy and temperature of the material. The equation for the enthalpy method account for heat conduction only and is one where basic energy conservation is applied to each element in the material. According to the enthalpy formulation,

$$\rho \frac{\partial h}{\partial t} = \nabla \cdot (k \nabla T) \tag{2.3}$$

where h is the enthalpy per unit mass and can be obtained from the following relation:

$$h = \begin{cases} C_{p,so} T & T < T_{so} \quad \text{solid phase} \\ C_{p,in}\, T + \dfrac{L(T - T_{so})}{(T_l - T_{so})} & T_s \leq T \leq T_l \quad \text{melting/solidification} \\ C_{p,l} T + (T_l - T_{so}) C_{p,in} + L & T \geq T_l \quad \text{liquid phase} \end{cases} \tag{2.4}$$

Equation (2.3) can be discretized and solved numerically. The enthalpy method has an advantage of not requiring an explicit tracking of the melting front which requires more complex deforming grids for analysis. Furthermore, this formulation is suitable for the development of in-house numerical codes using common software languages like MATLAB and FORTRAN, when the convection in the PCM could be neglected and a multi-dimensional problem could be simplified using reasonable assumptions [54]. It has been reported that the enthalpy method could give solution oscillations if the ratio of latent heat to sensible heat is large, however, the solution does not depend on the time step chosen or phase change temperature [57]. Bony and Citherlet [58]

validated a numerical model using the enthalpy method to predict the transient temperature at various positions inside a PCM module which was inserted into a water tank. Their model improved the basic enthalpy formulation by applying an effective thermal conductivity to account for natural convection within the PCM. The result indicated a significant improvement in the prediction as compared with the experiment. The model is currently being implemented in a TRNSYS type of water tank storage. The concept of effective thermal conductivity can also be applied to take into consideration enhancements such as forced convection, conductive fins, nanotubes, particles and other additives to improve the accuracy of the numerical solution [39].

In the enthalpy-porosity approach, the liquid-solid 'mushy zone' is treated as a porous zone with porosity equal to the liquid fraction, f, after which a source term is added to the momentum equation to account for the pressure drop in the region. The momentum equation is given by,

$$\rho \frac{D\boldsymbol{u}}{Dt} = -\nabla p + \mu \nabla^2 \boldsymbol{u} + \rho \boldsymbol{g} + \boldsymbol{S} \tag{2.5}$$

where $\boldsymbol{S}$ is the momentum source term and $\boldsymbol{u}$ is the velocity vector. In the momentum equation, the source term is given by,

$$\boldsymbol{S} = -\frac{C(1-f)^2}{(f^3+\varepsilon)} \cdot \boldsymbol{u} \tag{2.6}$$

where ε is a small number to avoid division by zero and C is another constant to reflect the nature of the mushy zone which usually ranges from 10^5 to 10^8 for most PCMs. The higher the value, the steeper the transition of the material velocity to zero as it

solidifies [54]. Contrary to the basic enthalpy formulation which only considers conduction in the PCM, the momentum equation in Equation (2.5) can be simultaneously solved with the energy and continuity equation to determine the flow field in the PCM, thereby taking natural convection into account. The enthalpy-porosity approach is used in commercial software like ANSYS Fluent to solve problems involving melting and solidification.

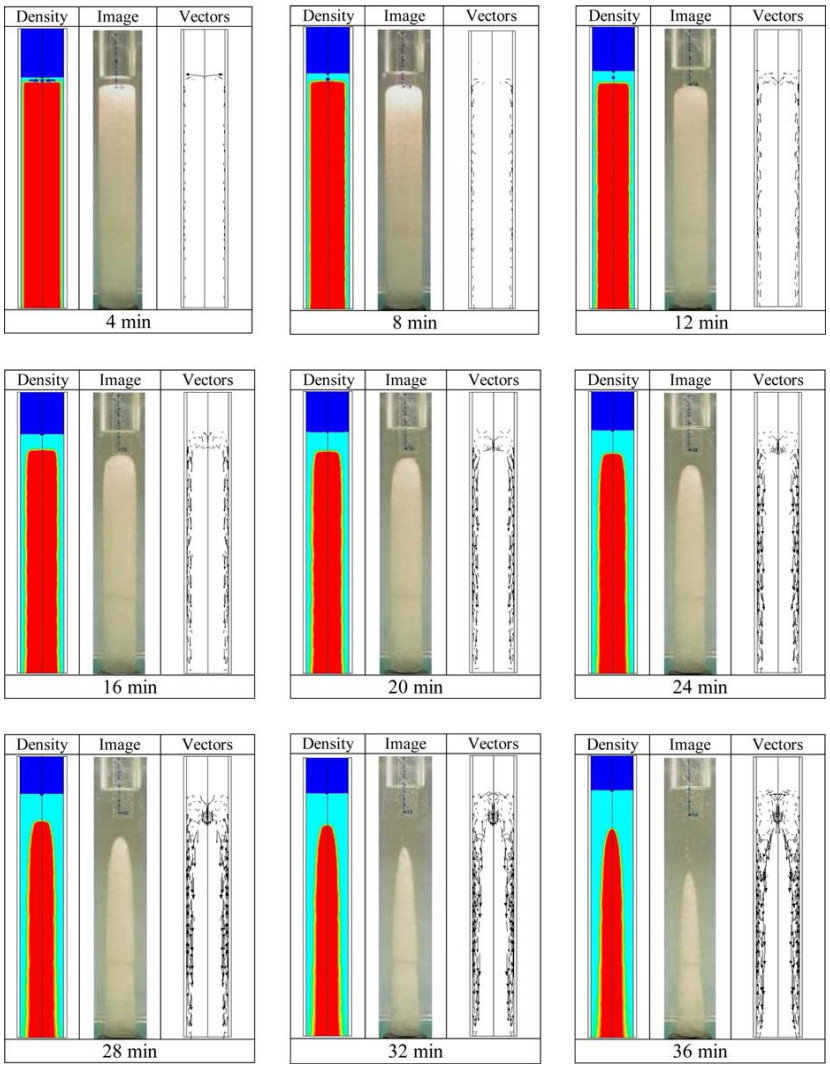

Figure 2.6: Experimental and numerical comparison of melting in a vertical cylindrical tube using enthalpy-porosity and VOF models with solid phase in red colour and liquid phase in cyan. Reprinted from [59], Copyright (2010) with permission from Elsevier.

A volume-of-fluid (VOF) model can be used in conjunction with the enthalpy-porosity approach in Fluent to model volume change due to the melting or solidification of the PCM. Shmueli et al. [59] performed a numerical investigation on melting of PCM in a vertical cylindrical tube and compared the results obtained with experiments as shown in Figure 2.6 which showed very good agreement. They reported that at the beginning of the melting process, the heat transfer was predominantly by conduction from the cylindrical surface to the PCM solid phases, but convection dominated the latter part of the melting process, which resulted in changing the solid phase to a shrunk conical shape.

2.6 Heat loss phenomena in biodiesel storage tanks

The study of heat loss in storage tanks is of great importance in regions which experience cold ambient temperatures. During the winter months, it is common to experience temperatures below -25°C, which is significantly below the cloud point or pour point of most biodiesel fuels, in places like Winnipeg, Canada. Most literature studies of heat loss in storage tanks have focused on applications like storage of temperature sensitive fluids like waxy crude oil and thermal energy storage in fluids like water or molten salts for domestic hot water or concentrated solar plants. However, a study of the transient cooling of a storage tank filled with biodiesel has not been reported in literature. Notwithstanding, biodiesel, just like most fluids will exhibit Newtonian behaviour at temperatures above the cloud point when yield stress

is expected to begin to develop. Therefore, a literature review of the transient heat loss phenomena in similar fluids is necessary.

The process of heat loss in tanks is a transient phenomenon and involves various modes of heat transfer. Within the fluid contained in the tank, the heat transfer is dominated by conduction and natural convection. Natural convection dominates at the initial stage of cooling, but with time the fluids become more viscous and inhibits convection leading to conduction dominating the heat loss process [60]. For higher temperature fluids like molten salts used in CSP applications, radiation from the fluid's free surface to the surrounding tank walls is significant and must be considered in the heat loss analysis [61]. Even though the heat loss by conduction can be orders of magnitudes lower than that of convection at lower oil temperatures, subsequent unloading of the tank becomes problematic when its temperature is below its pour point. For fuels like biodiesel, this would create problems in the fuel lines and engine filters; therefore, it is important to be able to predict the rate at which the fluid in a tank will cool under specified conditions.

The simplest approach to modelling the transient cooling of a fluid in a tank is assuming the fluid to be consisted of a well-mixed core enclosed by boundary-layer flow by the side wall due to natural convection effect. If the tank is insulated, the external resistance from the insulation and external convection can be assumed to be fixed, however, the internal resistance which depends on the boundary-layer varies with time and should be evaluated at every instant. Cotter and Charles [60] used a correlation of Nusselt number versus modified Rayleigh number obtained

numerically to evaluate the instantaneous internal heat transfer coefficient at the crude oil tank sidewall. The internal and external heat transfer coefficients were then used to calculate an overall heat transfer coefficient from which the transient average tank temperature was predicted using the energy balance relation,

$$\frac{T - T_{amb}}{T^t - T_{amb}} = exp\left\{-\frac{U_s A_s + U_b A_b + U_w A_w}{mC_p} \cdot \Delta t\right\} \tag{2.7}$$

where T^t is the temperature of the previous timestep, T_{amb} is the ambient temperature, Δt is the timestep, and the subscripts s, b and w refers to the free surface, bottom and sidewall respectively. Their well-mixed core oil tank model predicted the average transient temperature of cooling oil in a 60 m diameter tank, which showed excellent agreement with that predicted by a more sophisticated natural convection simulator which was presented in [62]. The overall heat transfer coefficient can also be determined experimentally, by considering the cooling rate of the fluid in the tank along with its thermal and physical properties. Even though the well-mixed tank model does not give a detailed solution of the spatial temperature profile in the tank, it is a useful method to determine the overall performance of a tank as it does not require large computational time due to its simplicity.

The more complex CFD approach to modelling heat loss in tanks involves the use of an appropriate numerical discretization scheme to solve the governing mass, momentum and energy conservation equations in the fluid. Density variation due to convection can be accounted for using the Boussinesq approximation, and a

temperature dependent viscosity function for the fluid can be introduced to improve the accuracy of the solution.

Most CFD studies on natural convection heat loss in tanks are performed in two-dimensional models with appropriate boundary conditions applied at the fluid surfaces to reduce computational time. Oliveski et al. [63] validated experimentally a numerical code developed to simulate natural convection within a cylindrical tank containing thermal oil. The wall temperature profile obtained from their experimental study was fed into the numerical program as a boundary condition. They also investigated the formation and degradation of thermal stratification within the oil tank and the result of their analysis indicated that the stratification increased and attained its maximum at 3 hours of cooling after which it began to deteriorate. While thermal stratification is a desired phenomenon for hot water storage tanks, it could pose a problem for biodiesel storages as the bottom of the tank would attain the CP much earlier during the cooling process and potentially clog the exit port of the tank. Therefore, appropriate measure should be taken to ensure a more uniform temperature in biodiesel tanks.

Cabeza et al. [64] reported that adding a suitable PCM to a TES or sensible heat storage fluid not only improves the energy capacity but also has an influence on the overall temperature characteristics during discharging. Ramana et al. [65] investigated the stratification performance of a storage tank with filled with PCM encapsulated spherical capsules. The result showed that there was enhancement in the stratification of the fluid in the tank as a result of the PCM addition. This was

evidently because the packed bed of PCM capsules was installed at the midsection of the tank resulting in a sharp thermocline at the midsection due to natural convection of the fluid. It is due to this reason that several researchers like Cabeza et al. [64] and Kumar et al. [66] are currently investigating the use of PCMs at the top of tanks to improve thermal stratification for domestic hot water applications. However, a different approach must be taken with the implementation of PCMs in biodiesel tank designs to prevent or minimize a sharp thermocline which would pose problems for the diesel engine operation; but no current study addresses this issue.

3

Experimental and numerical methodology

To demonstrate the benefits of implementing PCM in fuel tanks, an experimental and numerical investigation were carried out. However, for the experimental investigation, canola oil was used instead of B100 biodiesel to validate the concept. Canola oil was used as a replacement due to safety restrictions on conducting tests using certain volumes of flammable fluids within the University of Manitoba refrigerated wind tunnel. For temperatures above the cloud point, B100 biodiesel, like many other fluids, behaves as a Newtonian fluid and will have similar thermal behaviour as canola oil. Therefore, characterizing the thermal behaviour of canola oil in a tank containing PCM pencils would be an efficient tool to predict the behaviour of B100 biodiesel above cloud point given that its physical properties are known. A numerical model is used which accurately predicts the experimental results and the same model can be used to simulate the performance of biodiesel using its properties without having to conduct additional experiments or build tanks with different geometries.

3.1 Experimental methodology

The setup for the experiment as shown in Figure 3.1 consists of a 381×381×485 mm aluminium tank shell, a stainless-steel heat exchange tube with insulated feed and return lines. Materials used for the tank construction were carefully selected due to compatibility issues with B100 biodiesel with some materials. The aluminium tank is placed in a custom wooden crate made of Oriented Strand Board (OSB) which contains extruded polystyrene insulation which was cut into shape to fit into the crate. Insulation of 2.7 inches thickness and R-value of 13.5 was used around all sides of the tank. The tank top contains 12 holes of diameter 58 mm through which the removable PCM pencils are inserted and one 95 mm hole at the centre where the heat exchange tube is installed. The PCM pencils consist of 50.8 mm OD aluminium tubes welded to a flange through which the pencil is bolted to the tank top.

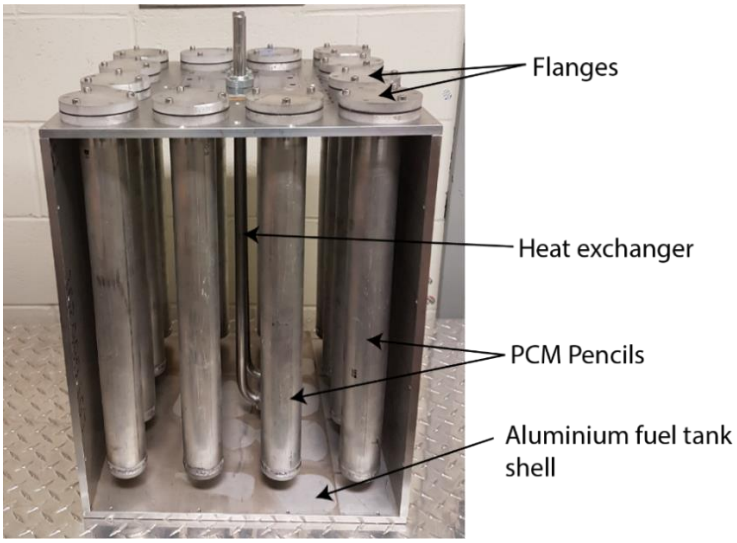

Figure 3.1: Picture showing the internal components of the tank before final assembly.

The tubes are each filled with 0.65 litres of RT18HC organic PCM obtained commercially from Rubitherm GmbH with melting point between 17 and 19˚C. Other properties of the commercially available PCM can be found in Table 3.1 and its partial enthalpy (sum of sensible and latent energy) distribution is shown in Figure 3.2.

Table 3.1: Properties of Rubitherm RT18HC PCM [67]

Property	Value
Liquid phase density (kg/m^3)	770
Solid phase density (kg/m^3)	880
Solidification temperature (˚C)	17
Melting temperature (˚C)	19
Specific heat capacity (J/kgK)	2000
Heat storage capacity (kJ/kg)	260
Volume expansion (%)	12.5
Thermal conductivity (W/mK)	0.2

Temperature measurements were collected using 4 T-type profiling thermocouples with six measurement points each separated by 1.75 inches along the length. Two of the thermocouples were placed to measure the oil temperature and the other two were used to measure the temperature of the PCM in the pencils as shown in Figure 3.3.

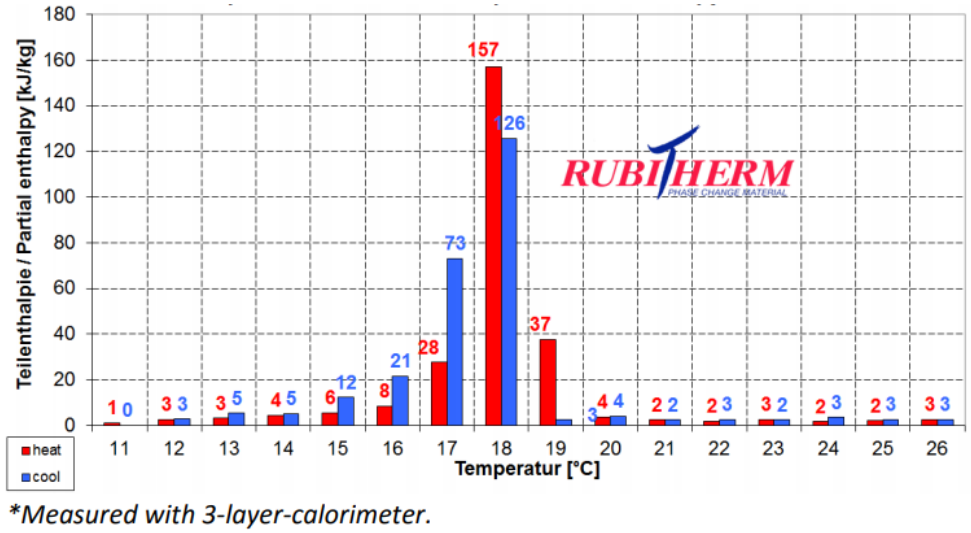

Figure 3.2: Partial enthalpy distribution for Rubitherm RT18HC PCM obtained from the manufacturer.

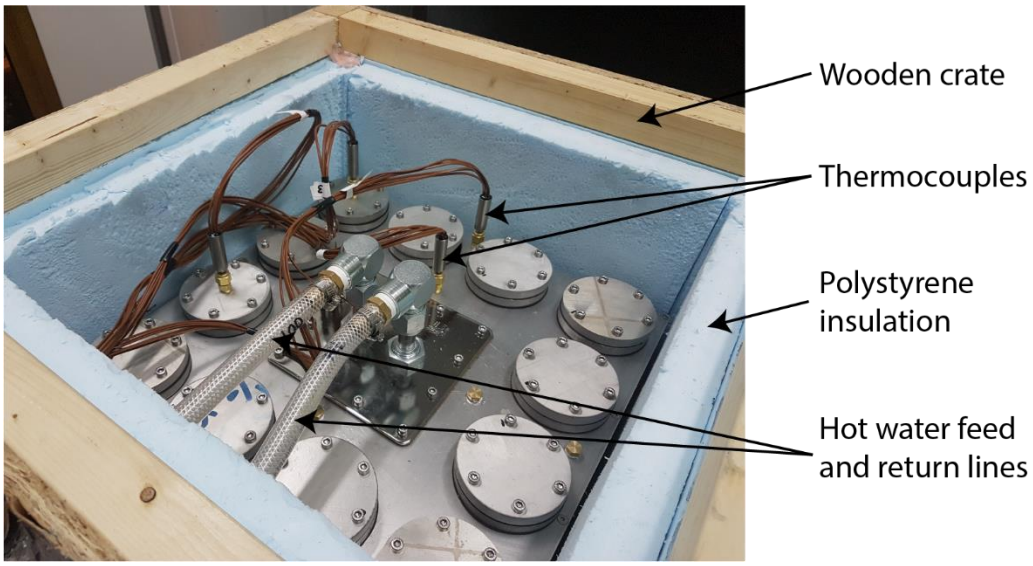

Figure 3.3: Top of the test tanks showing the instrumentation, insulation and hot water feed and return lines.

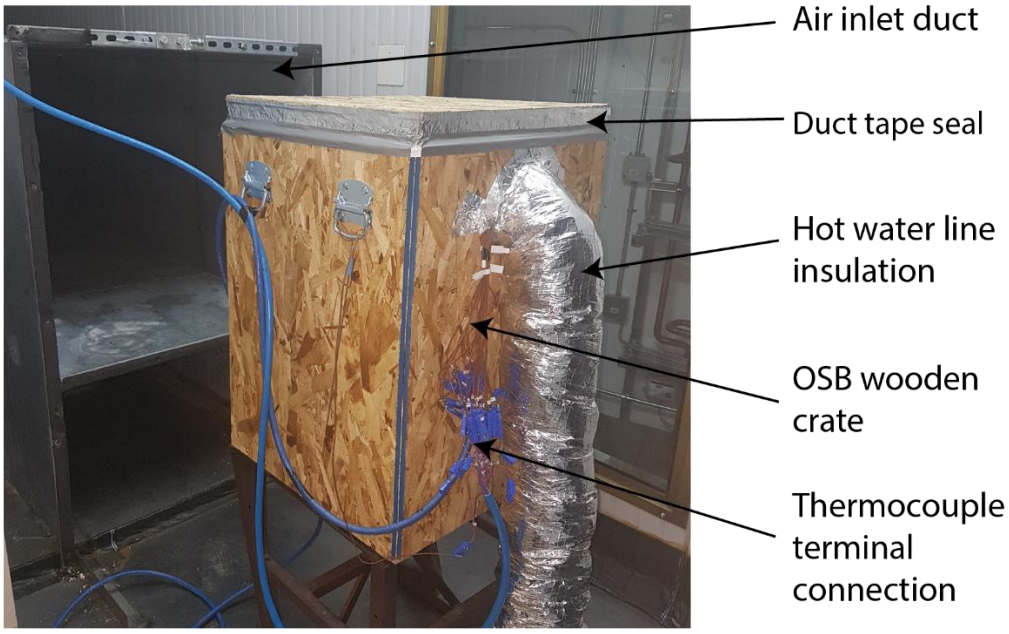

Figure 3.4: Tank setup in the icing tunnel.

The test with setup shown in Figure 3.4 was done in the icing tunnel facility at the Thermofluids lab of the University of Manitoba. During each test, the icing tunnel was set to an average ambient temperature of -20˚C and a wind speed of 10 m/s. The volume of oil contained in the tank in each case was 33.2 litres. Without the PCM pencils inserted, the fluid height of the oil in the tank was 9 inches (229 mm).

The tests were conducted to record the transient temperature drop of the canola oil from an initial temperature of 20℃ to a final temperature of 5℃ (an assumed cloud point) under the above stated ambient conditions. Three tests were carried out by varying the number of PCM pencils in the tank as shown in Table 3.2. Due to the addition of the pencils, the resulting increase in tank weight and loss of volume are also reported in the Table. The positioning of the PCM pencils for Tests 2 and 3 are

shown in Figure 3.5 with the red circles. Figure 3.5 also shows a representation of the thermocouple positioning in the oil and PCM pencils for each of the tests carried out.

Table 3.2: Varied test parameters for experiment

Experiment	Number of PCM tubes	Increase in tank weight (%)	Loss of volume (%)
Test 1	None	None	None
Test 2	4	29.5	5.2
Test 3	12	88.5	15.7

Test 1 was used both as a control experiment and to determine the overall heat coefficient of the tank using Equation (3.7) shown later in the section. This is due to the method used to assemble the insulation into the wooden box, of which using the R-value of the insulation in calculation would result in erroneous results due to the heat leakages expected from the joints of the assembly.

In all test conditions, the oil was heated up by passing hot water at 40°C through the heat exchangers until the temperature of the fluid in the tank rose to approximately 25˚C after which the hot water supply was turned off. Water was used for testing purposes, whereas in actual diesel engine implementation, the hot fluid providing the heat would be the ethylene-glycol coolant connected to the tank as demonstrated in Figure 1.7. The temperature of the oil in the tank was then allowed to drop until a temperature of 5˚C was attained. A data taker, model DT90, stored the transient

temperatures from the thermocouples in the tank at a one-minute interval from the initial temperature to final temperature.

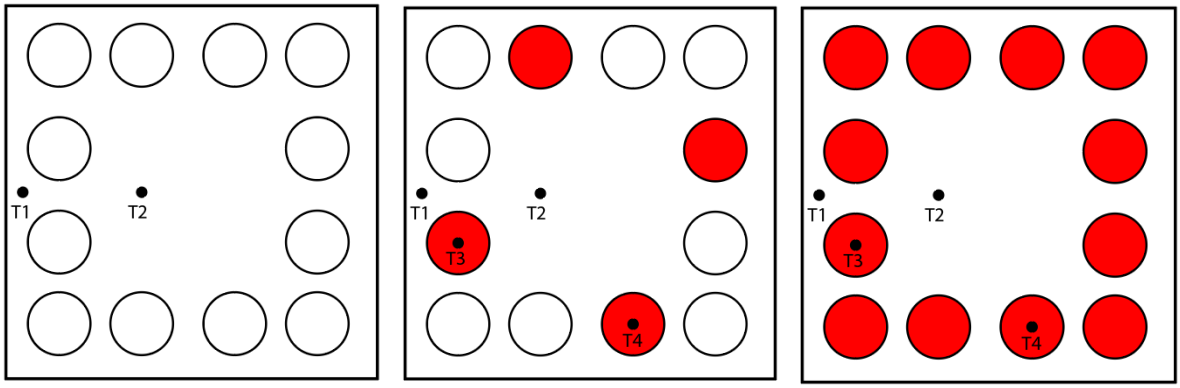

Figure 3.5: Positioning of the PCM tubes (red colour) and thermocouples for oil and PCM temperature measurements: Test 1 (left), Test 2 (middle), and Test 3 (right).

The average oil temperature was taken as the mean of the immersed measurement points of thermocouples T1 and T2 which were placed close to the wall and the bulk of the fluid respectively, while that of the PCM was taken as the mean of temperatures from T3 and T4.

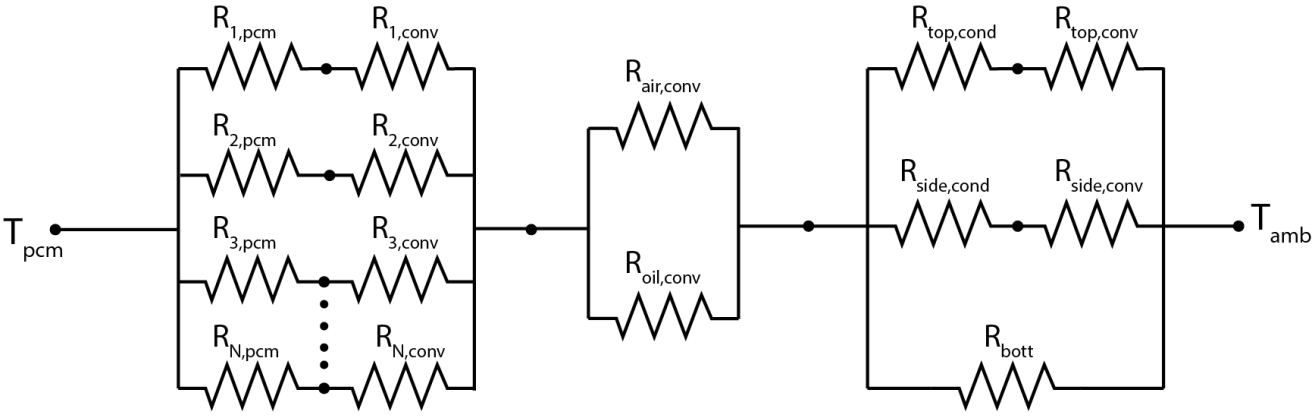

Figure 3.6: Thermal resistance network of the biodiesel fuel tank setup

It should be noted that the purpose of this tank design was exclusively for validation purposes. While the concept remains essentially the same, the geometry of the tank used does not reflect the actual design to be implemented in diesel truck tanks. The thermal resistance network of the biodiesel tank setup is presented in Figure 3.6. The diagram shows the flow of heat from the PCM pencils to the oil and air, and finally the heat is lost through the top, side and bottom of the tank as a result of the lower ambient temperature.

3.2 Numerical methodology

A numerical model was developed using MATLAB to approximate the results obtained experimentally. It was also necessary to develop a numerical model since canola oil was used in the experiment so that the performance of actual biodiesel tanks could be predicted by the simulation by specifying biodiesel properties as inputs to the program. To develop the program, certain assumptions were made to reduce the complexity of the problem without significantly sacrificing the accuracy of the solution. Some of the assumptions made in the MATLAB model are outlined below:

1. Temperature variations of the oil in the tank is neglected and only an average oil temperature is used.
2. Heat transfer in the PCM is assumed to be by conduction only. However, convection within the PCM tube is accounted for by utilizing an 'effective thermal conductivity' as will be discussed later in the sections.

3. Due to the assumption of a uniform average oil temperature, heat transfer to and from the PCM is assumed to be only in the radial direction. Therefore, all cylindrical planes along the height of the PCM tubes will have the same temperature profile. Consequently, only the submerged height of the PCM is considered for the heat transfer analysis.
4. An overall heat transfer coefficient is used to account for the insulation, internal and external convection of the oil tank. Therefore, the top, side and bottom of the tank are assumed to have a constant overall heat transfer coefficient during the period of heat loss.
5. Sub-cooling and hysteresis effects in the PCM are not considered.
6. The heat transfer between the top air zone and the oil is neglected.

By considering these assumptions, equations were derived using a finite difference method by applying energy conservation at each node of the PCM and the oil and an explicit method was used to calculate the transient temperature of the oil.

Figure 3.7 shows the schematic of the PCM in the oil tank. An enthalpy method is used in the whole model to calculate the temperatures. By performing an energy conservation on the oil, it follows that:

$$\dot{Q}_{oil} = \dot{Q}_{pcm} + \dot{Q}_{loss} \tag{3.1}$$

where $\dot{Q}_{pcm}$ and $\dot{Q}_{loss}$ are the rate of heat transferred by the PCM pencils and the rate of heat loss to the ambient respectively. At any instant, the heat transfer by PCM can be calculated by:

$$\dot{Q}_{pcm} = N h_{pcm} A_{pcm} (T_{pcm,con} - T_{oil}) \tag{3.2}$$

where N is the number of PCM pencils in the tank, h_{pcm} is the coefficient of heat transfer from PCM container to oil, A_{pcm} is the wetted area of the PCM pencils, and $T_{pcm,con}$ is the temperature of the PCM container.

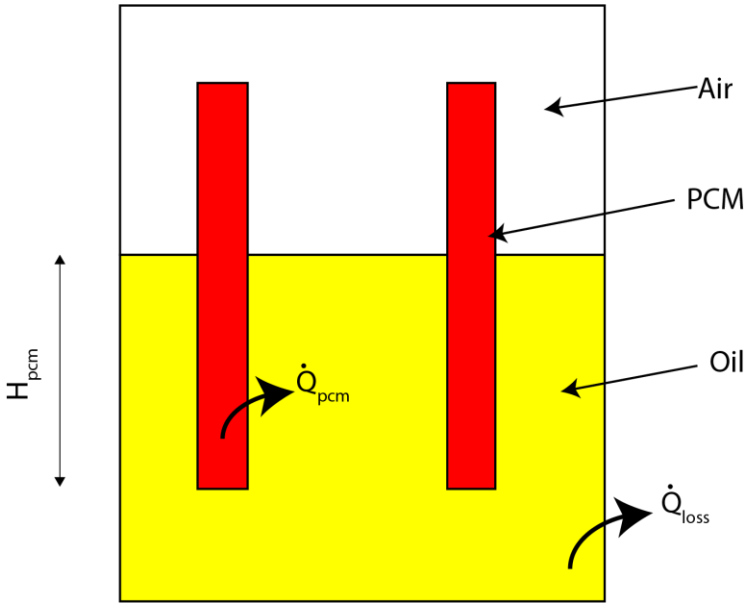

Figure 3.7: Schematic representation of PCM in fuel tank.

The instantaneous value of h_{pcm} can be calculated using the popular correlation for natural convection on a vertical plate for Rayleigh number ranging from 10^{-1} to 10^{12} [68].

$$Nu = \left\{ 0.825 + \frac{0.387 Ra^{1/6}}{\left[1 + \left(\frac{0.492}{Pr}\right)^{9/16}\right]^{8/27}} \right\}^2 \tag{3.3}$$

Considering the characteristic length, H_{pcm}, as the wetted height of the PCM tubes it follows that,

$$h_{pcm} = Nu \frac{k_{oil}}{H_{pcm}} \tag{3.4}$$

The heat loss from the tank can also be calculated using,

$$\dot{Q}_{loss} = UA_{st}(T_{amb} - T_{oil}) \tag{3.5}$$

where U is the overall heat transfer coefficient of the tank and A_{st} is the total heat loss surface area of the oil which is the sum of the areas of oil free surface, tank bottom and wetted tank side wall.

For an insulated tank the overall heat transfer coefficient can be calculated using the resistances of the insulation and the external heat transfer coefficient as shown in Equation (3.6)

$$R = \frac{1}{U} = \frac{1}{h_i} + \frac{t}{k_{ins}} + \frac{1}{h_e} \tag{3.6}$$

where t and k_{ins} are the thickness and thermal conductivity of the insulation and h_i and h_e are respectively the internal and the external heat transfer coefficient of the tank. It should be noted that this overall resistance implicitly takes into account the natural convection effect in the oil through the internal heat transfer coefficient, h_i. Literature review shows that for common practical situations, the value of h_e ranges from 9.5 to 11 W/m^{2}K [69]. However, these differences are subdued as the greatest resistance comes from the insulation resistance. Alternatively, the overall heat transfer coefficient can be determined experimentally (in a tank without PCM pencils inserted) for arbitrary geometries or setups with imperfect insulations where the use of Equation (3.6) would be inaccurate. This can be achieved by using the properties

of the fluid and assuming a constant rate of temperature decay in the oil as in Equation (3.7).

$$U = \frac{(mC_p)_{oil}\dfrac{T_{oil}^1 - T_{oil}^2}{t_d}}{A_{st}\left(\dfrac{T_{oil}^1 + T_{oil}^2}{2} - T_{amb}\right)} \tag{3.7}$$

where T_{oil}^1, T_{oil}^2, and t_d are the initial oil average temperature, final oil average temperature and time for temperature decay respectively.

Referencing back to energy conservation in the oil, it follows that:

$$\dot{Q}_{oil} = m_{oil}\frac{dh_{oil}}{dt} \tag{3.8}$$

Consequently, the transient oil enthalpy can be calculated by,

$$h_{oil}^{t+1} = h_{oil}^{t} + \frac{\dot{Q}_{oil}^{t}\Delta t}{(\rho V)_{oil}} \tag{3.9}$$

The time $t + 1$ and t represent the values at the new and old time respectively, while Δt is the time step chosen for the problem.

To determine the transient PCM temperature, the enthalpy method is also used. From the partial enthalpy distribution data shown in Figure 3.2, a temperature-enthalpy curve is produced as shown in Figure 3.8. The temperature at every time step is calculated by calculating the enthalpy of the PCM and interpolating for the temperature using the curve.

Bony and Citherlet [70] improved the accuracy of their PCM modelling by using an effective conductivity to account for convection in the PCM defined as follows [71]:

$$k_{eff} = k_{pcm} Nu_{pcm} \tag{3.10}$$

Where Nu_{pcm} can be calculated for H/D ranging from 1 to 40 as,

$$Nu_{pcm} = 0.046 Ra^{1/3} \tag{3.11}$$

This equation is valid for Rayleigh number ranging from 10^6 to 10^9. It should be noted that the Rayleigh number is calculated using the temperature difference between the PCM centre node and the PCM container.

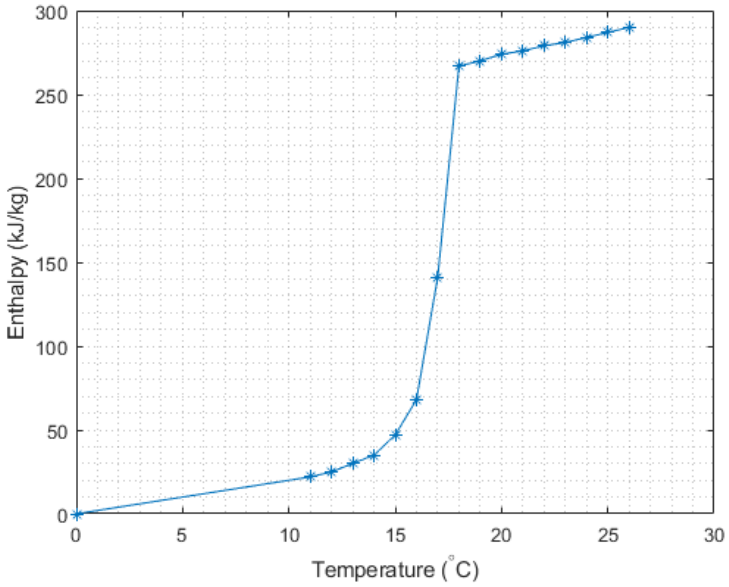

Figure 3.8: Enthalpy-temperature curve for Rubitherm RT18HC PCM.

With reference to Figure 3.9, the temperature distribution in the PCM at every time can be obtained by discretizing the PCM domain into n radial nodes. Therefore, the size of each node is:

$$dr = \frac{R_i}{n} \tag{3.12}$$

where R_i is the internal radius of the PCM pencil.

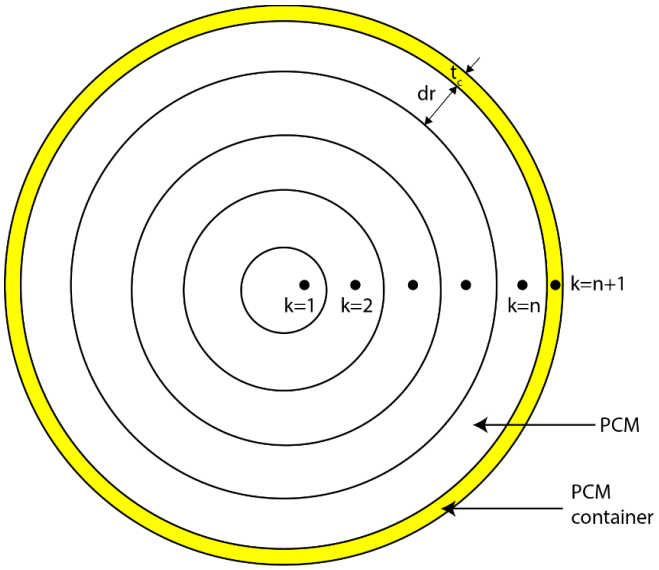

Figure 3.9: Discretization of PCM and PCM container for finite difference solution.

The equation for each discrete node, k, have been derived and are presented as follows,

For the centre PCM node ($k = 1$):

$$h_1^{t+1} = h_1^t + \frac{k_{eff} A_{2\to1} (T_2^t - T_1^t)}{m_1 dr} \Delta t \tag{3.13}$$

For the interior PCM nodes ($k = 2$ *to* $n-1$):

$$h_k^{t+1} = h_k^t + \frac{k_{eff} A_{k+1\to k} (T_{k+1}^t - T_k^t)}{m_k dr} \Delta t + \frac{k_{eff} A_{k-1\to k} (T_{k-1}^t - T_k^t)}{m_k dr} \Delta t \tag{3.14}$$

For the last PCM node ($k = n$):

Due to the difference in the conductivities of PCM and the container, an interface thermal conductivity should be defined.

$$k_{int} = \frac{k_{eff} k_{con}}{w \cdot k_{eff} + (1 - w) k_{con}} \tag{3.15}$$

Where k_{con} is the thermal conductivity of the PCM container and w is the grid weight at the interface defined by,

$$w = \frac{t_{con}}{t_{con} + dr} \tag{3.16}$$

It then follows that,

$$h_n^{t+1} = h_n^t + \frac{k_{eff} A_{n-1 \to n} (T_{n-1}^t - T_n^t)}{m_n dr} \Delta t + \frac{k_{int} A_{n+1 \to n} (T_{n+1}^t - T_n^t)}{m_n (r_{n+1} - r_n)} \Delta t \tag{3.17}$$

For the PCM container ($k = n + 1$):

$$h_{n+1}^{t+1} = h_{n+1}^t + \frac{k_{int} A_{n \to n+1} (T_n^t - T_{n+1}^t)}{m_{n+1} (r_{n+1} - r_n)} \Delta t + \frac{h_{pcm}^t A_{n+1} (T_{oil}^t - T_{n+1}^t)}{m_{n+1}} \Delta t \tag{3.18}$$

Since an explicit method is used to obtain the solution, it is important to define a maximum timestep to be used to prevent divergence. The maximum timestep is therefore evaluated at the convective boundary of the PCM container as,

$$\Delta t \leq \frac{C_{p,n+1} m_{n+1} (r_{n+1} - r_n)}{k_{int} A_{n \to n+1} + h_{pcm}^t A_{n+1} (r_{n+1} - r_n)} \tag{3.19}$$

which can be simplified as:

$$\Delta t \leq \frac{(C_p \rho V)_{con} (t_c/2 + dr/2)}{k_{int} A_{i,con} + h_{pcm}^t A_{e,con} (t_c/2 + dr/2)} \tag{3.20}$$

where $A_{i,con}$ and $A_{e,con}$ are the internal and external wetted surface area of the PCM container and $(C_p \rho V)_{con}$ represents the thermal capacity of the wetted height of the PCM container in Joules per Kelvin.

After several test simulations for grid independence and numerical stability, the calculations were performed using a timestep of one second, seven radial nodes in the PCM and one node in the PCM container.

The properties of the canola oil used in the simulations as presented in Table 3.3 are obtained from Reference [72]. This reference also contains more detailed data on the effect of temperature on the density and kinematic viscosity of the fluid.

3.3 Detailed visualization study using ANSYS Fluent

For visualization of the PCM solidification process and temperature stratification in oil tanks, a more detailed CFD analysis was conducted using ANSYS Fluent for a sample case of a tank with a single PCM pencil inserted. A full-scale analysis (tank with multiple PCM pencils) was not considered due to the computational effort and time required to simulate such a transient problem in 3D. Note that this case was not for direct comparison to the experimental result or MATLAB model described in the preceding section, but solely for visualization study.

Table 3.3: Properties of canola oil at 20°C [72]

Parameter	Value
Density (kg/m^3)	920
Specific heat capacity (kJ/kgK)	1910
Thermal conductivity (W/mK)	0.2
Dynamic viscosity (kg/ms)	0.07147

For the numerical model, two cases are studied. In the first case, shown in Figure 3.10(left), the tank contains only the biodiesel sample, while in the second case, shown in Figure 3.10(right), there is a tube of PCM inserted into the cylindrical insulated biodiesel tank. The increased biodiesel tank height due to the presence of the PCM tube in the second case is accounted for to ensure the volume of the biodiesel is constant at 4.06 litres in both test scenarios.

For the both cases, the different zones indicated in Figure 3.10 are setup in Ansys Fluent with the energy equation and solidification and melting model activated for the tank with PCM. To further simplify the simulation and save sufficient computing time, the cylindrical tank was simulated in 2D using an axisymmetric boundary condition at the centre of the tank.

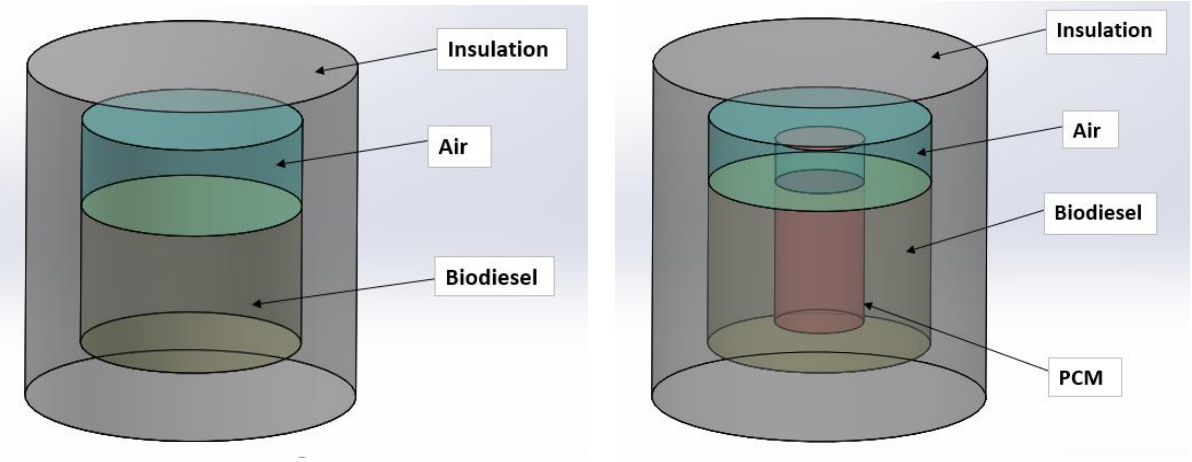

Figure 3.10: 3D geometry representation of the cases used for the numerical modelling: tank without PCM (left), and tank with PCM inserted (right).

Other assumptions made in this model are as follows:

1. The cloud point of the B100 biodiesel used for the simulation is 5˚C, which is a typical value for biodiesel.
2. Viscosity and specific heat capacity changes with temperature for both biodiesel, air and PCM are assumed to be insignificant. Therefore, constant values were used.
3. Due to the relatively low temperature of the biodiesel in the tank, radiation heat transfer is considered negligible and heat loss from the tank is only by conduction and natural convection.
4. The ambient temperature around the tank is assumed to be constant at a value of -25˚C. This is considered a reasonable average winter temperature in cold regions like Winnipeg, Canada.
5. The bottom of the tank is also assumed to be maintained at a constant temperature of -25˚C which is typical of tank placed on a flat surface in the ambient in winter.
6. Heat transfer coefficient from the tank to the air is 12 W/m^2K which is a conservative case compared to that used in literature. For example, values of 10, 11 and 9.5 have been used by different authors in accordance with common practical situations [73].

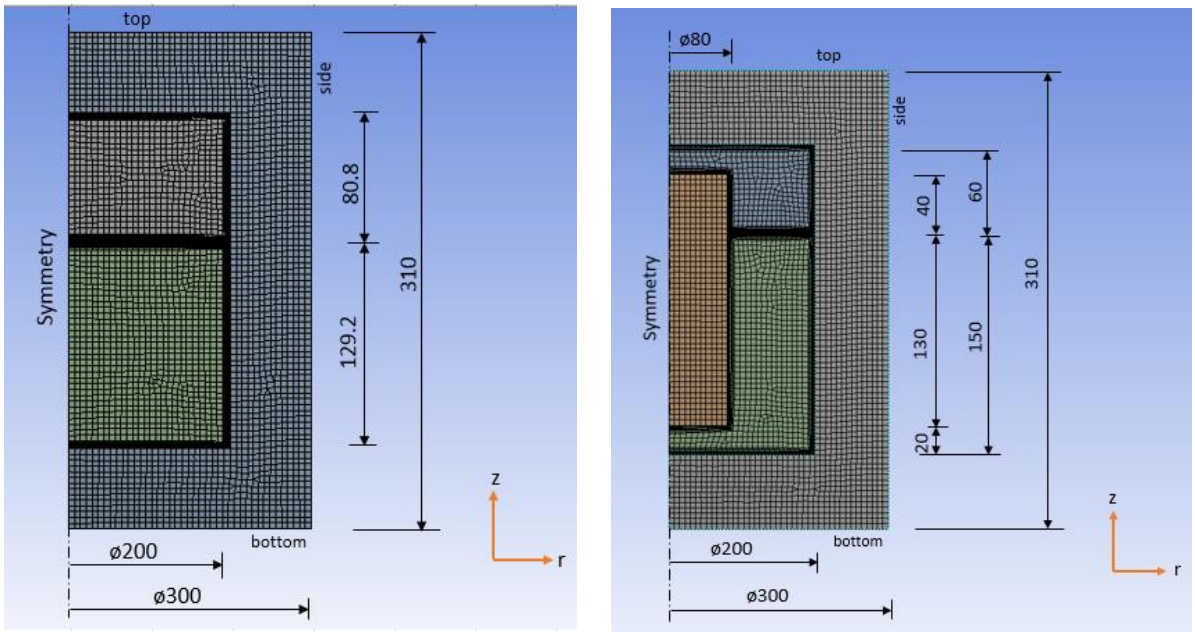

Figure 3.11: 2D meshing of both cases simulated showing smaller sized nodes (inflation layers) near the wall to resolve the boundary layer: tank without PCM (left), and tank with PCM (right). Dimensions are in mm.

The Boussinesq model was used to simulate the natural convection in the air and biodiesel zones by specifying their coefficient of thermal expansion. The coefficient of thermal expansion of air was calculated based on that of ideal gases at specified temperature while the value used for B100 biodiesel was obtained based on the correlation from the work of Santos et al. [74] for corn biodiesel. Other properties of the biodiesel used for the simulation are shown in Table 3.4

Figure 3.11 shows the meshing and dimensions used for both cases. The mesh sizes used near the wall interfaces with the fluids are smaller to resolve the boundary layer and give a more accurate numerical solution.

Table 3.4: Properties of B100 biodiesel used for the simulation in ANSYS Fluent

Property	Value
Density (kg/m^3)	884.319
Specific heat capacity (J/kgK)	2000
Thermal conductivity (W/mK)	0.149
Dynamic viscosity (kg/ms)	0.005216
Thermal expansion coefficient (K^{-1})	0.000839

4

Results and discussion

In this section, the results of the fuel tank experiments for the 3 tests with 0, 4 and 12 PCM containing pencils are presented. Afterwards, comparisons are made with the numerical results obtained using the method highlighted in the previous chapter. The trends observed in these results are discussed and the numerical model is further used to simulate different conditions to study the impact on the tank performance.

4.1 No PCM in tank

As stated in the previous section, the test with no PCM in the tank was conducted to serve both as a control experiment for comparison and to determine the tank's overall heat loss coefficient using Equation (3.7). The equation was used with the properties of canola oil as presented in Table 3.3 and the overall heat loss coefficient, U, was calculated as 0.62 W/m^{2}K. This calculated value was used to showcase the transient

average temperature for the oil using a relation obtained from the energy balance for the oil volume as shown in Equation (4.1) using the well-mixed tank model.

$$T_{oil}^{t+1} = \left(1 - \frac{UA_{st}\Delta t}{(mC_p)_{oil}}\right) T_{oil}^{t} + \left(\frac{UA_{st}\Delta t}{(mC_p)_{oil}}\right) T_{amb} \qquad (4.1)$$

The comparison of the numerical and experimental results shown in Figure 4.1 indicates a very good match even though a constant temperature decay rate was used in the estimation of the overall heat transfer coefficient. Therefore, given the satisfactory nature of the assumption made, a constant value was used for the remaining numerical calculations.

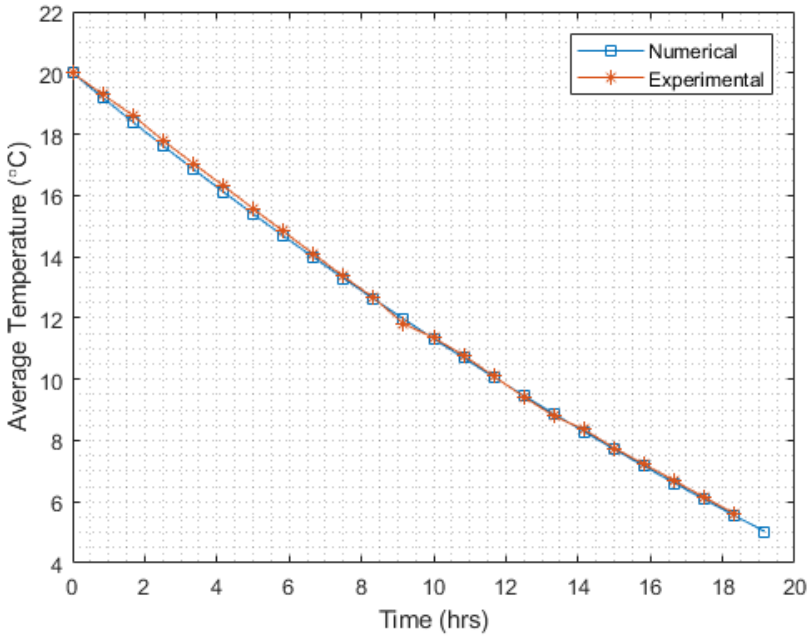

Figure 4.1: Experimental and numerical transient average oil temperature for tank without PCM inserted.

Other parameters important for the simulation are shown in Table 4.1 below.

Table 4.1: Tank parameters for numerical calculation of transient heat loss

Parameter	Value
Tank heat loss area	0.6393 m^2
Tank Fluid height	0.229 m
Tank overall heat transfer coefficient	0.62 W/m^2K

The experimental results showed that it took the oil 18.6 hours for the temperature to drop from 20℃ to 5℃, while the numerical result predicted it took 19.2 hours for the same temperature range.

4.2 Tank with PCM pencils inserted

The volume of PCM in each container as stated in the last section was 0.65 litres. With the internal diameter of the PCM container as 44.45 mm the PCM height in each tube was calculated as 418.8 mm. However, this entire height is not considered to be engaged in heat transfer with the oil in the tank. The only portion for heat transfer with the oil is the submerged portion of the tube as the numerical model assumes that the portion above the oil is involved in an isolated heat transfer with the surrounding air for simplification.

4.2.1 4 PCM containers in tank

The experimental results showed that it took the oil 22.5 hours to fall from 20℃ to 5℃ with the addition of 4 PCM pencils as shown in Figure 4.2. This indicated an

improvement by 21% in the time above cloud point. The figure also shows a comparison of the experimental results with the numerical model formulated and shows good agreement. Analysis of the result indicated a maximum temperature difference of 0.6℃ between the numerical and experimental data. This implies that the simplified model can be used to predict the performance of tanks with PCM inserted with significant accuracy. Overall, the numerical model predicted that the oil takes 23 hours to drop to the assumed cloud point of 5℃.

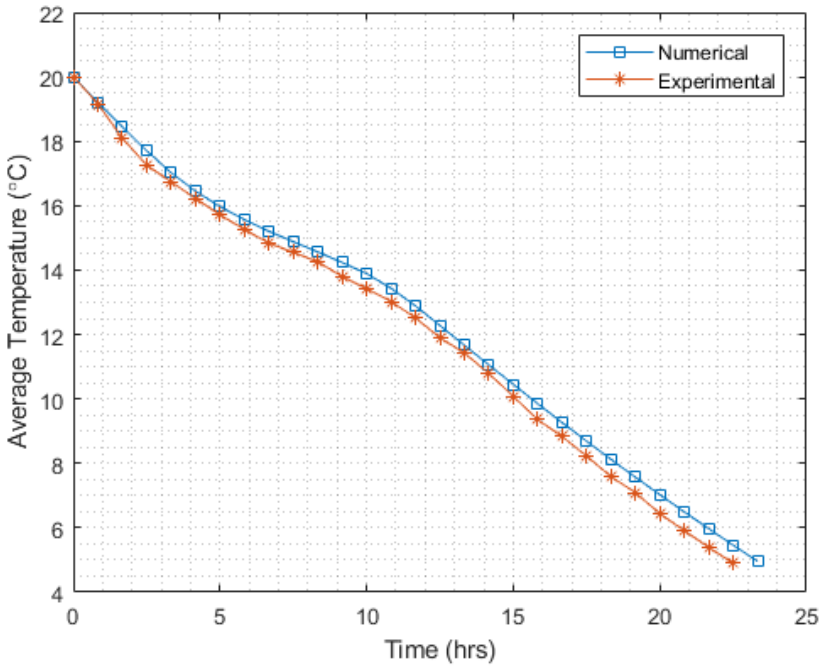

Figure 4.2: Experimental and numerical transient oil temperatures for tank with 4 PCM tubes inserted.

Table 4.2 shows the parameters used in the MATLAB simulation. Comparison with Table 4.1 for the tank without the PCM pencils indicate an increase in the tank fluid height and heat loss area. This can be explained by the volume displacement of the

oil due to the introduction of the PCM pencils in the tank. The increase in fluid height results in an increase in the tank sidewall heat transfer. The heat loss area at the free surface of the oil is also reduced by the introduction of the PCM pencils, but calculations indicate that the addition of new PCM pencils results in a net overall increase in the oil heat loss surface area.

Close observation of Figure 4.2 shows the period of phase change begins at about 2.5 hours as indicated by a reduction in the cooling rate. This is because the temperature of the PCM remains relatively constant during the phase change period and acts as a heat source to the oil. Therefore, the heat transfer between the PCM and the oil by the release of stored latent energy compensates for the heat loss of the oil to the ambient. At about 12 hours, the cooling rate increases again and this indicates when the latent energy in the PCM is exhausted and only sensible heat transfer takes place.

Table 4.2: Parameters for tank with 4 PCM pencils inserted

Parameter	Value
Tank heat loss area	0.6491 m^2
Tank fluid height	0.241 m
PCM wetted height	0.201 m
Tank overall heat transfer coefficient	0.62 W/m^2K

4.2.2 12 PCM containers in the tank

With 12 PCM pencils in the tank, the experimental results show that the time above cloud point was increased to 33 hours, a 77.4% increase from the case of the tank

without the PCM. As earlier highlighted, the inclusion of more PCM pencils in the tank results in oil volume displacement which leads to increasing the height of oil in the tank. The increase in the height of oil with each additional PCM pencil added also increases the wetted contact area between the oil and the PCM, thereby making more PCM available for heat transfer with the oil.

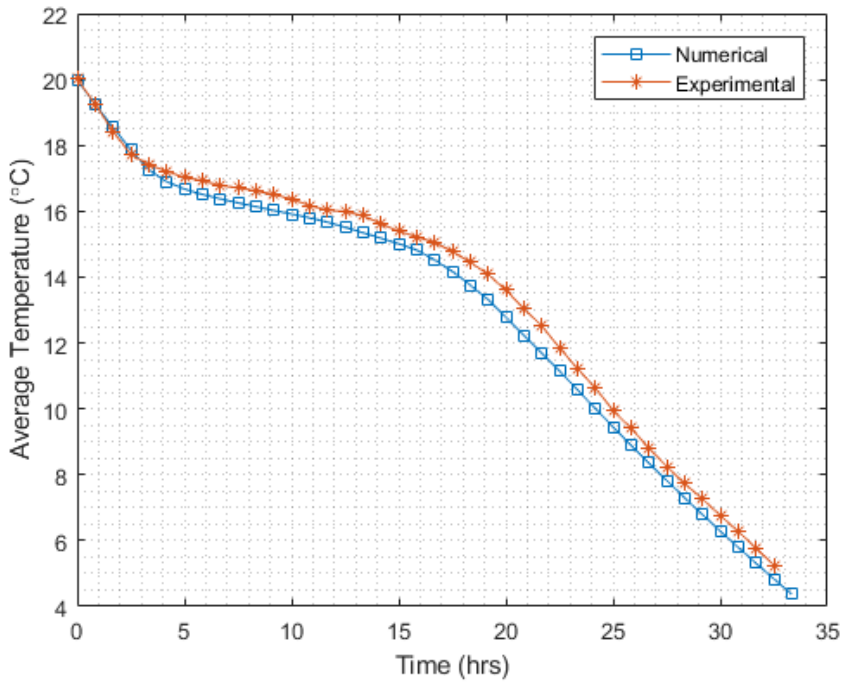

Figure 4.3: Experimental and numerical transient oil temperature for tank with 12 PCM tubes inserted.

The numerical simulation for 12 tubes conducted using the parameters shown in Table 4.3 also shows good agreement with the experimental result. The numerical model predicts that it takes the oil 32.3 hours to attain the temperature of 5°C. As is expected the addition of more pencils significantly slows down the cooling rate between 2.5 and 17.5 hours after which the cooling rate increases again. The

maximum temperature difference between the experimental and numerical results was approximately 1°C which shows the model is also validated for predicting a system with higher number of pencils with good accuracy.

Table 4.3: Parameters for tank with 4 PCM pencils inserted

Parameter	Value
Tank heat loss area	0.6759 m^2
Tank fluid height	0.269 m
PCM wetted height	0.229 m
Tank overall heat transfer coefficient	0.62 W/m^2K

4.3 Effect of varying number of PCM pencils on tank performance

The PCM serves as thermal batteries in the tank, therefore, the effect of adding more PCM pencils in the tank will be to extend the duration of the oil above cloud point as earlier shown by the experimental results presented in Section 4.2. For a clearer comparison, of the benefits of implementing PCM in the tank design, numerical simulations were performed for cases with 2, 6, 10, 14 and 18 tubes inserted in the tank. Figure 4.4 illustrates the effect of increasing the number of PCM pencils in a tank containing 33.18 litres of oil in each case similar to the experiments. The results indicate that using as much as 18 PCM tubes in the tank could potentially increase the time above cloud point by 114% relative to the case without the PCM.

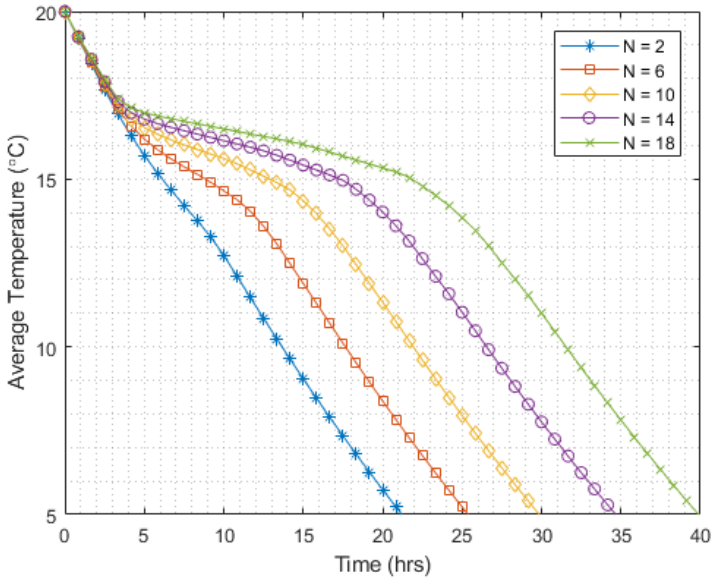

Figure 4.4: Effect of various number of PCM pencils (N) on the tank performance

Table 4.4 shows the parameters used for the numerical simulation while Figure 4.5 shows a plot of number of pencil versus the time above cloud point which indicates an approximate linear relationship.

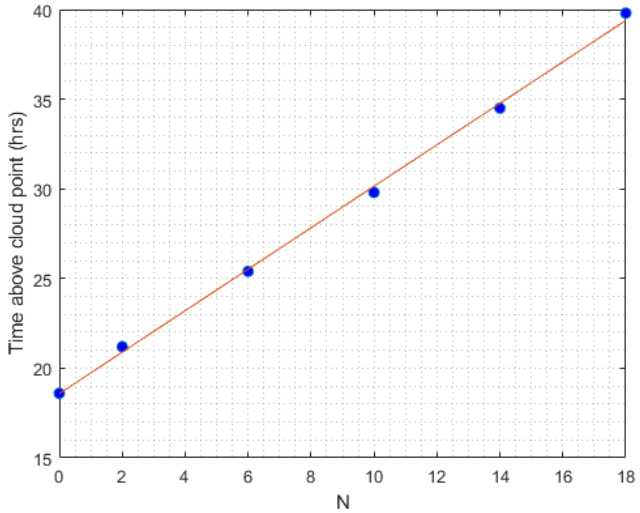

Figure 4.5: Plot showing an approximate linear relationship between number of PCM pencils and time above cloud point.

On further analysis, it is also observed that the incremental time gain becomes higher as the number of PCM pencils increases. This is because the fluid level in the tank becomes higher and there is more wetted area involved in the heat transfer between the PCM and oil.

Table 4.4: Tank parameters for various numbers of PCM pencils simulated

N	Tank wetted height, H_{st} (m)	PCM wetted height H_{pcm} (m)	Tank heat loss area A_{st} (m²)
2	0.2347	0.1946	0.6440
6	0.2471	0.2070	0.6548
10	0.2612	0.2211	0.6681
14	0.2772	0.2371	0.6844
18	0.2956	0.2555	0.7043

Despite the benefit gained by including more PCM pencils in the tank, a potential disadvantage is that the volume it occupies will result in reduced fuel volume that can be accommodated in the tank. Therefore, a compromise would have to be reached between the number of PCM pencils for the application and the fuel capacity of the tank. Table 4.5 shows the percentage of tank volume occupied by including various number of PCM modules in the tank.

Table 4.5: Benefits of using varied number of PCM pencils in tank

N	Time above cloud point, t_c (hrs)	Incremental time addition (hrs)	Tank space occupied by PCM tubes (%)
0	18.6	0.0	0.0
2	21.2	2.6	2.6
6	25.4	4.2	7.8
10	29.8	4.4	13.1
14	34.5	4.7	18.3
18	39.8	5.3	23.5

4.4 Effect of varying PCM pencil diameter on tank performance

To investigate the impact of using a larger or smaller diameter of PCM pencils on the tank performance, the PCM pencil diameter is varied while keeping the total submerged volume constant. This allows for a uniform comparison since the same volume of PCM is involved in the heat transfer process. The implication of using a larger or smaller diameter PCM pencil while maintaining the same volume is that fewer or more PCM tubes respectively are used in the tank. New internal and external diameters were calculated for 2, 4, and 12 PCM tubes and compared to a base scenario of 8 PCM tubes with internal diameter of 44.45 mm and external diameter of 50.80 mm (the same specification for the experiment). The following equation was used to calculate the new diameters in each case.

$$D_{i,2} = D_{i,1}\left(\frac{N_1}{N_2}\right)^{1/2} \tag{4.2}$$

$$D_{e,2} = D_{e,1}\left(\frac{N_1}{N_2}\right)^{1/2} \tag{4.3}$$

where D_i and D_e are the PCM pencil internal and external diameter, N is the number of PCM pencils and the subscript 1 and 2 represent the initial and final values. To preserve the accuracy of the calculation, the number of nodes in the PCM has been changed correspondingly when the diameters were changed. Figure 4.6 shows the impact of changing the PCM diameter on the tank performance. The result shows that in the long term, the time above cloud point is independent of the diameter of the PCM pencil.

The comparison of the four cases indicate difference in the temperature of the oil mainly during the phase change period where the oil cooling rate is lower. Increasing the diameter of the pencils have an effect of a lower oil temperature during the phase change period and vice versa. This is because a larger diameter decreases the overall contact surface area which reduces the power delivered by the PCM during the phase change period, whereby using a smaller diameter has the opposite effect.

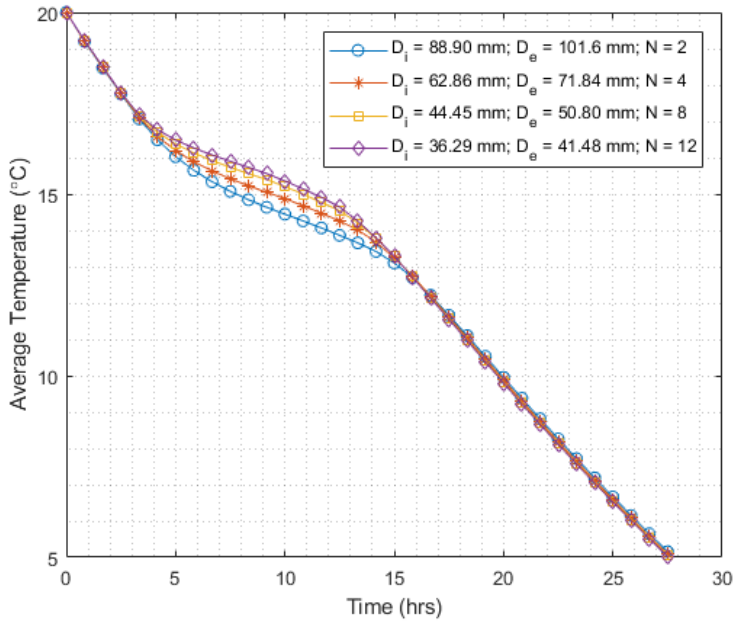

Figure 4.6: Effect of change in PCM pencil diameter on tank performance

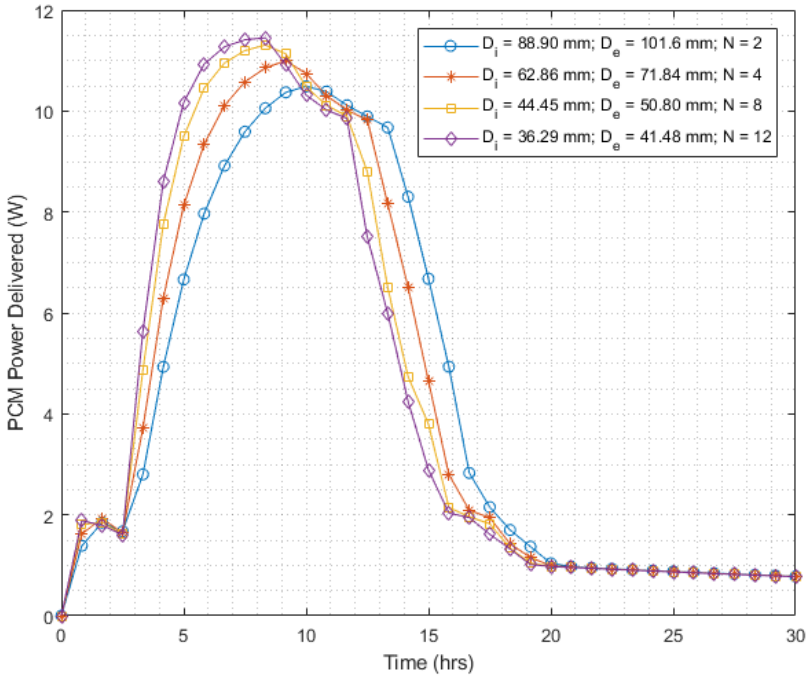

Figure 4.7: Power delivered by the PCM pencils for various tube diameters

Figure 4.7 further illustrates how the PCM delivers power to the oil during the entire process. All cases in the plot have similar profiles. Early in the process the power delivered by the PCM is lower because the oil and PCM are at approximately the same temperature since only sensible heat is lost. At about 2.5 hours, the phase change process begins where the PCM temperature remains relatively constant. During this period, the oil temperature cools at a lower rate and as the oil temperature drops, the temperature difference with reference to the PCM increases leading to a higher power delivery. After the latent energy in the PCM is exhausted, the power delivery starts to drop until the PCM attains approximately the same temperature as the oil. For the cases with smaller diameter, the PCM delivers the power at a faster rate which leads to an earlier depletion of the stored latent energy, and vice versa. This is the reason why the oil temperatures ultimately converge and is independent on the diameter of the PCM tubes in the long run.

4.5 Effect of overall heat transfer coefficient on tank performance

The effect of overall heat transfer coefficient, U, was investigated by performing five simulations for case of 12 PCM pencils in the tank, where the values were 0.2, 0.4, 0.6, 0.8 and 1.0 W/m^{2}K. The result is presented in Figure 4.8. The analysis of the plot shows that as the heat transfer coefficient decreases from 1.0 to 0.2 W/m^{2}K there is significant increase in the time above cloud point. Since the insulation represents the greatest thermal resistance and has the most influence on the overall heat coefficient, it shows that the tank performance is greatly impacted by the thickness or thermal

conductivity of the insulation chosen. Furthermore, great attention must be given to the insulation and sealing method to ensure that there are minimal heat leakages from the tank.

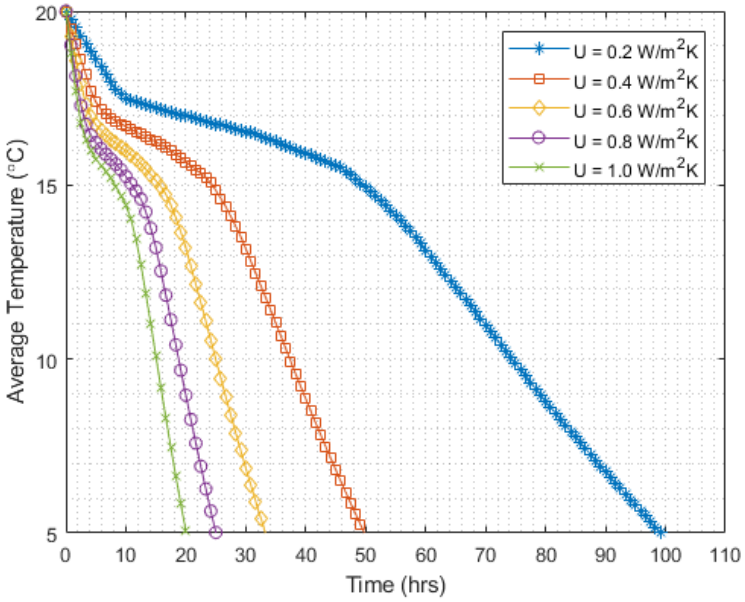

Figure 4.8: Effect of overall heat transfer coefficient on tank performance.

Using the numerical results obtained, it was found that a relationship could be obtained between the overall heat transfer coefficient and time above cloud point with 95% confidence as shown in Figure 4.9. The relationship was approximated using the power relation as follows,

$$t_c = 20U^{-0.994} \tag{4.4}$$

Even though the coefficients of the above relation are specific to the case presented, similar relations could be developed for different tanks and the coefficients would depend primarily on the properties of the fluid and the PCM used while the overall heat transfer coefficient would be an independent variable as in Equation (4.2).

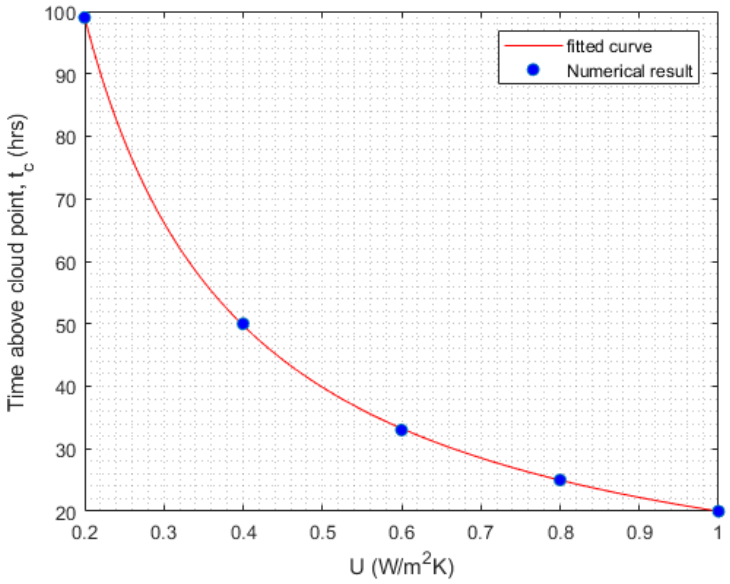

Figure 4.9: Relationship between overall heat transfer coefficient and time above cloud point. We assume 100 hours being acceptable for performance.

4.6 Effect of tank filling level on tank performance

It has earlier been established that the wetted height of the PCM is an important parameter because it determines the amount of PCM that engages in the heat transfer with the oil. As the oil volume in the tank is increased, the oil level rises and so does the heat transfer contact area with the PCM pencils and therefore results in an increase in the time above cloud point as is shown in Figure 4.10. A visual observation of the plot indicates that as the oil volume increases, the differential increase in time above cloud point becomes smaller. This is because increasing the tank volume not only increases the area of contact for heat transfer with the PCM,

but also increases the heat loss area of the oil to the ambient. The overall effect is higher heat losses from the oil as is reflected in the plot shown.

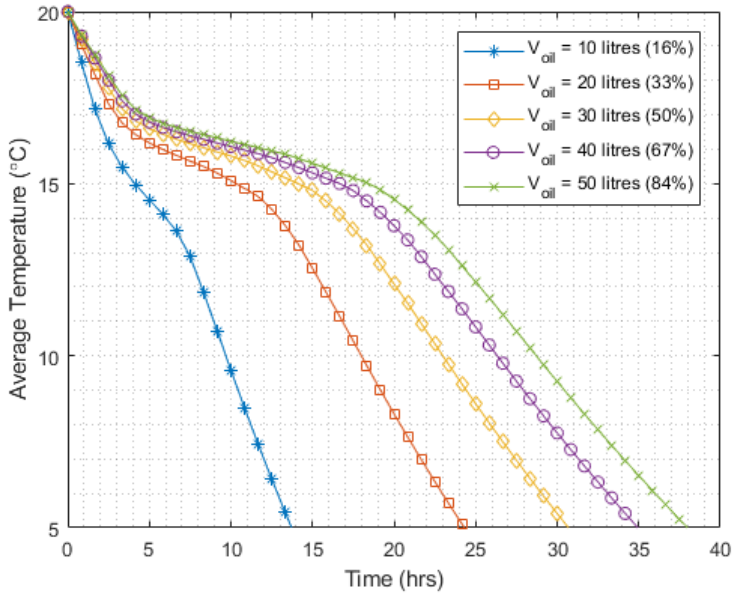

Figure 4.10: Tank performance for various oil levels

Nevertheless, it is important to note that maintaining the tank at a higher level helps to preserve the temperature above cloud point for longer periods.

Table 4.6 illustrates the benefits of higher oil volume (or level) by comparing to scenarios of tanks without PCM with time above cloud point, t_c^0, calculated using Equation (4.1). It shows that for higher tank volumes, there appears to be a limit on the improvement in tank performance (as demonstrated by percentage increase in time above cloud point) i.e. 68%, for a case with 12 PCM pencils in the tank due to the same reason earlier highlighted. This limiting value could be dependent on any combination of PCM properties, oil properties, insulation, tank geometry (aspect ratio), and number of PCM pencils.

Table 4.6: Comparison of tank performance with and without PCM pencils for varying oil volume (level).

Oil volume, V_{oil} (Litres)	t_c^0 (hrs) *No PCM*	t_c^{12} (hrs) *12 PCM tubes*	Improvement, Δt_c (%)
10	9.3	13.7	47.3
20	14.9	24.2	62.4
30	18.4	30.6	66.3
40	20.8	35.0	68.3
50	22.6	38.0	68.1

4.7 Problem analysis and visualization using ANSYS Fluent

The transient average temperature results from the simulation case described in Section 3.3 is presented in Figure 4.11. All zones in the numerical simulation were initialized to 20˚C (293.15 K). In an actual scenario, the biodiesel heater heats the fuel up to about 40˚C and the discharge begins around this temperature. Since the process of sensible heat loss from fluids is well established, and to save significant simulation time, the simulation is started at 20˚C where the phase change process is about to begin.

Figure 4.11(left) shows that it takes the B100 biodiesel 17.2 hours to drop from its initial temperature to the cloud point without the use of the PCM. However, as seen in Figure 4.11(right), when the PCM is used in the tank there is a significant increase in time by 338% to 75.3 hours.

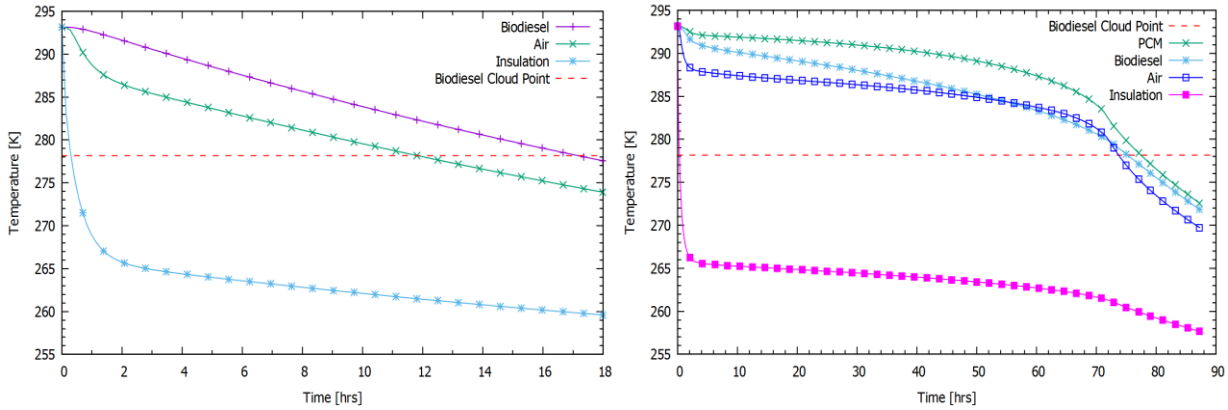

Figure 4.11: Transient temperatures for the different zones simulated in both cases: tank without PCM (left), and tank with PCM inserted (right).

The graph also shows the temperature of the air zone above the biodiesel is lower than that of the biodiesel for the entire simulation. The temperature of the air and of the insulation drops rapidly for the first two hours after which the cooling rate becomes relatively slow during after the system attains equilibrium. In Figure 4.11(right), the sharp drop in temperature for biodiesel, air, and insulation was also expectedly observed after the process of phase change in the PCM was completed at 17℃ (290.15 K).

Figure 4.12 shows the heat loss from the top, side and bottom walls of the tank for both cases investigated. The largest heat loss is through the tank side, while the top and the bottom approximately have the same heat loss. The higher heat loss from the side is due to the greater surface area and higher heat transfer coefficient for vertical cylindrical walls compared to the horizontal surfaces. The sharp drop in heat loss at the beginning of the simulations is due to the initial high temperature difference between the insulation surface and the ambient.

Figure 4.13 shows the contour of local temperature distribution in the biodiesel at the onset of clouding at 5°C (278.15 K). The results show that biodiesel clouding in both cases begin at the base of the tank. Thermal stratification can also be observed since there is no agitation of the fuel as is typical when trucks are left parked for extended periods in the winter. Comparison of the two cases show a higher thermal stratification in the tank with the PCM. This stratification was highest towards the base of the tank below the PCM. If the fuel exit port is below the tank, this could pose a problem due to the crystallization and eventual gelling formation below the tank. This phenomenon could be prevented by having the PCM pencils extend towards the base of the tank or a different design with PCM packed at the base of the tank.

At the start of the simulation, the PCM was in liquid phase as its temperature was above the melting temperature. Figure 4.14 shows the process of solidification of the PCM contained in the tank. A mass fraction of 1 represents a liquid phase while 0 represents a solid phase. The solidification process starts from the walls of the PCM tube and proceeds to the centre, as is shown in Figure 4.14(a) to (f).

The solidification process is also seen to be faster in the part of the PCM submerged in the biodiesel due to the higher rate of heat loss from the wetted area compared to the air-filled area above the free surface. The results also indicate that the solidification of the PCM is completed at 72 hours.

Figure 4.15 and Figure 4.16 shows the velocity contours and flow streamlines respectively in the biodiesel. A flow recirculation zone can be observed below the PCM tube shown in Figure 4.16 which results in inefficient convection heat transfer and

mixing of the fluid. Consequently, the oil at the base of the tank cools at a much faster rate than that at the top resulting in a very sharp thermocline just below the PCM tube.

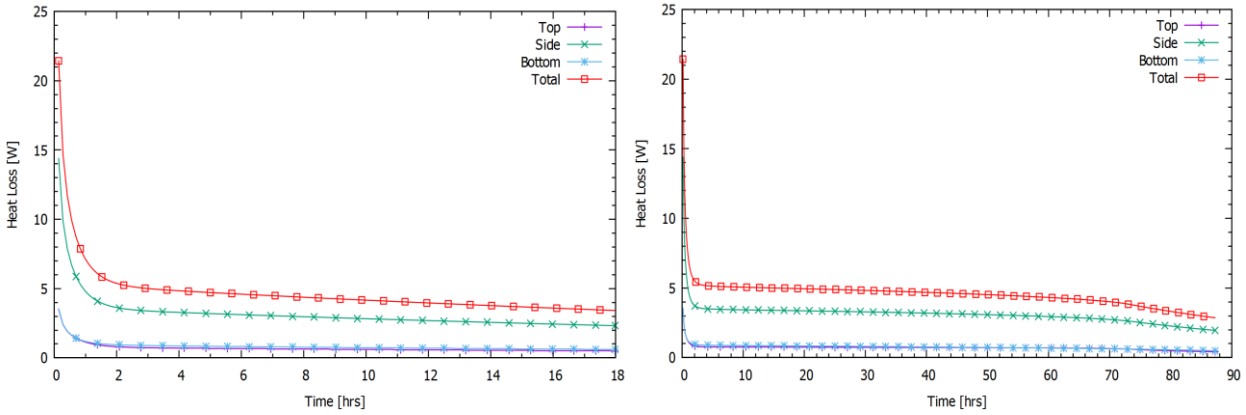

Figure 4.12: Heat loss from the top, side and bottom of the tank: tank without PCM (left), and tank with PCM inserted (right).

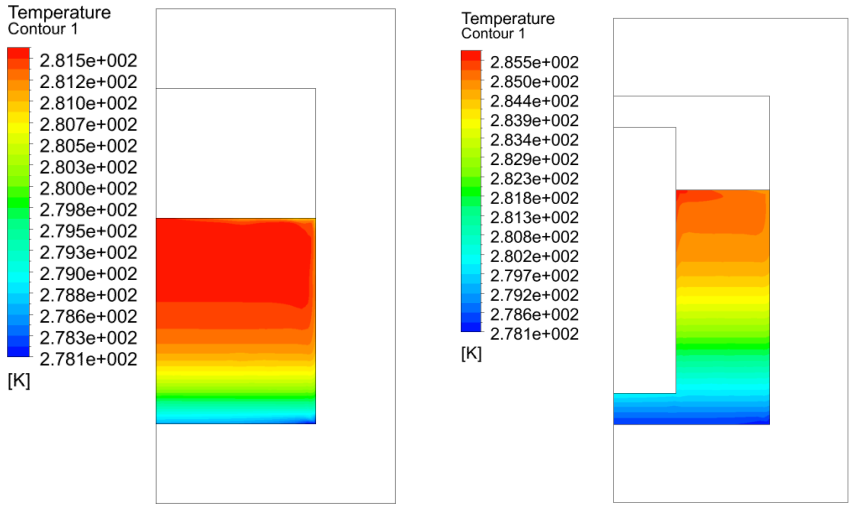

Figure 4.13: Temperature contours at the onset of clouding in the cases simulated: tank without PCM (left), and tank with PCM inserted (right).

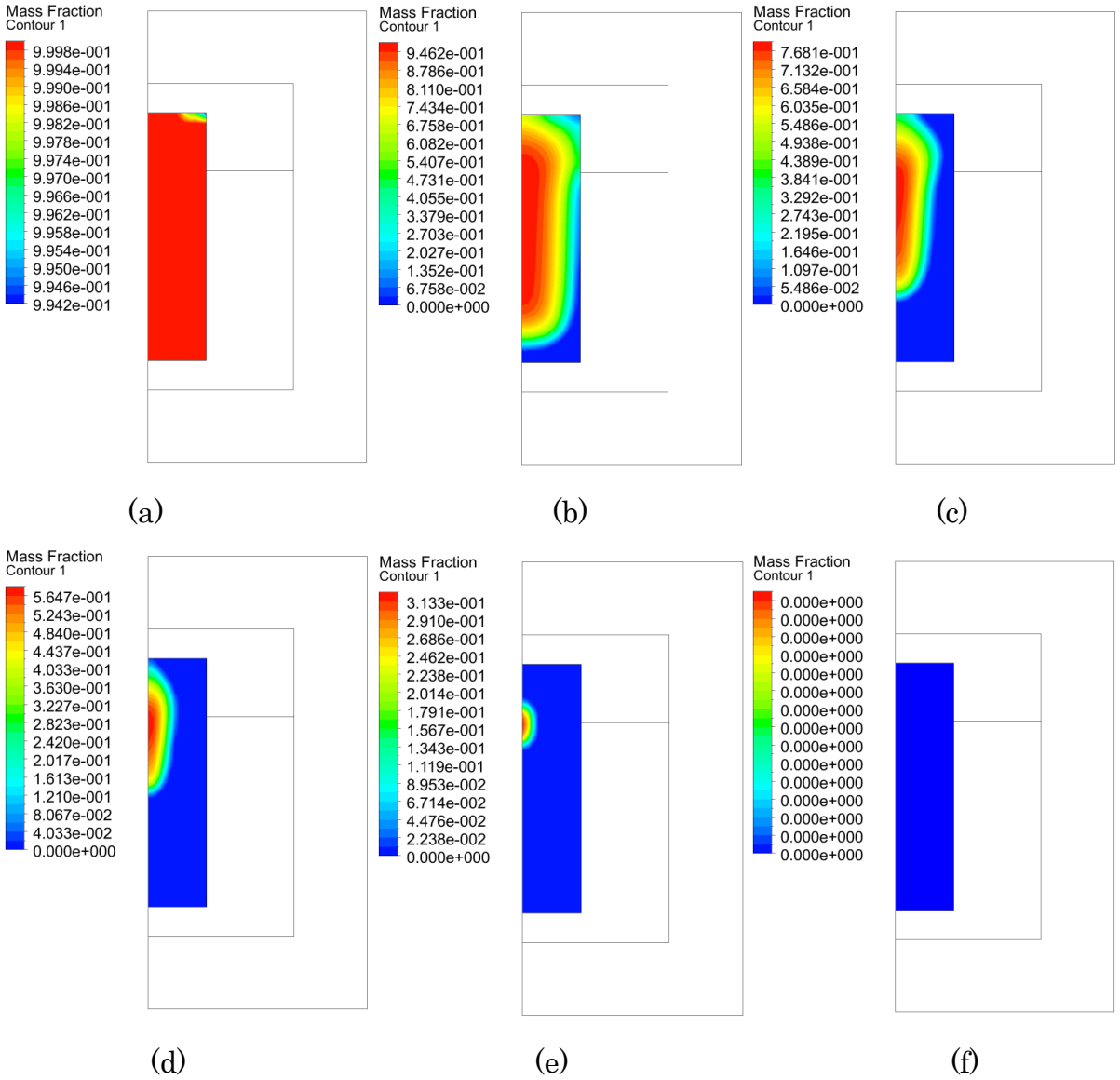

Figure 4.14: Liquid fraction of the PCM at different times between the phase change process from liquid (red colour) to solid (blue colour): (a) t = 1 hr, (b) t = 25 hrs, (c) t = 50 hrs, (d) t = 63 hrs, (e) t = 70 hrs, and (f) t = 72 hrs.

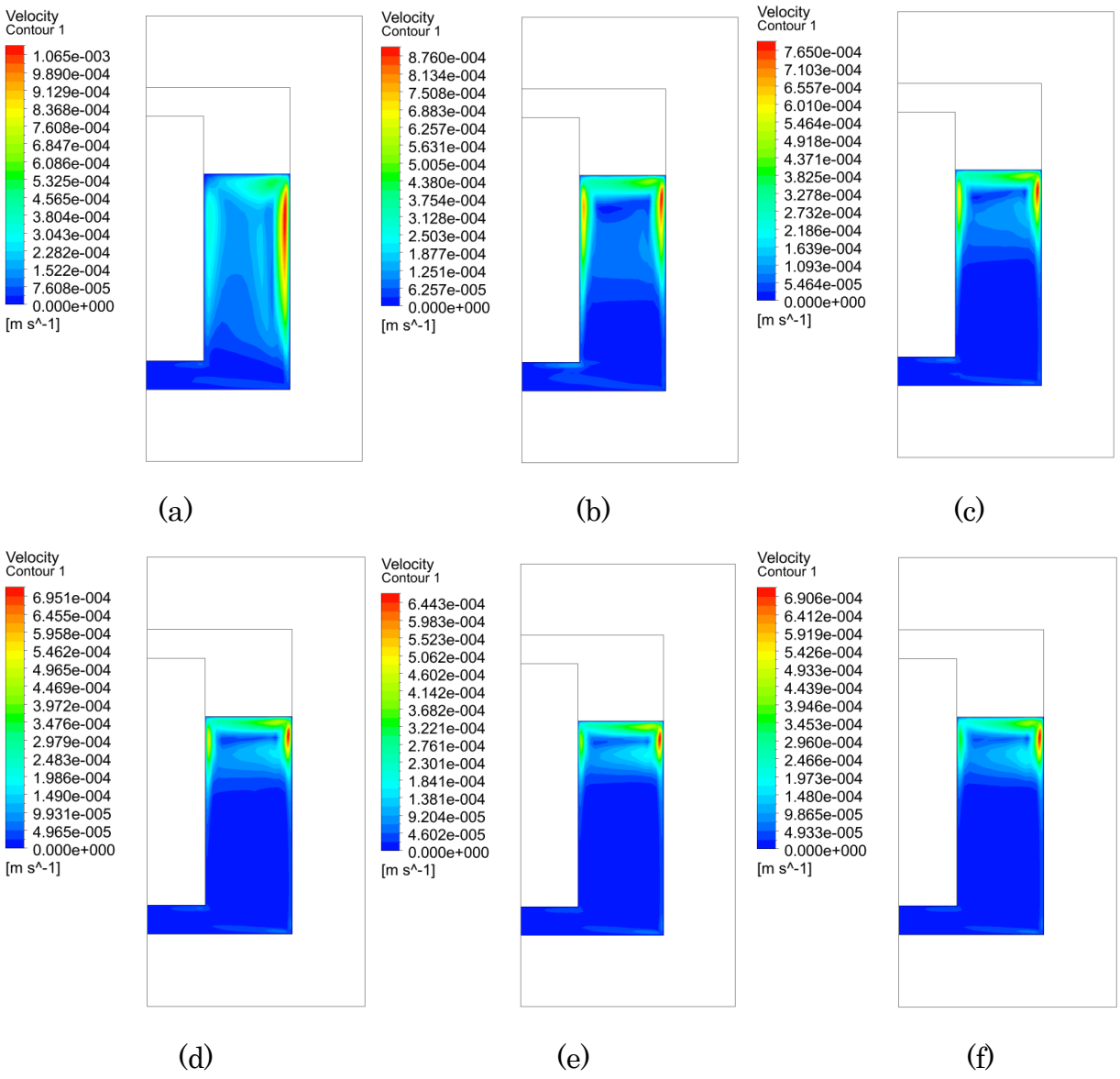

Figure 4.15: Velocity contours in the biodiesel at different times between the phase change process from liquid to solid: (a) t = 1 hr, (b) t = 25 hrs, (c) t = 50 hrs, (d) t = 63 hrs, (e) t = 70 hrs, and (f) t = 72 hrs.

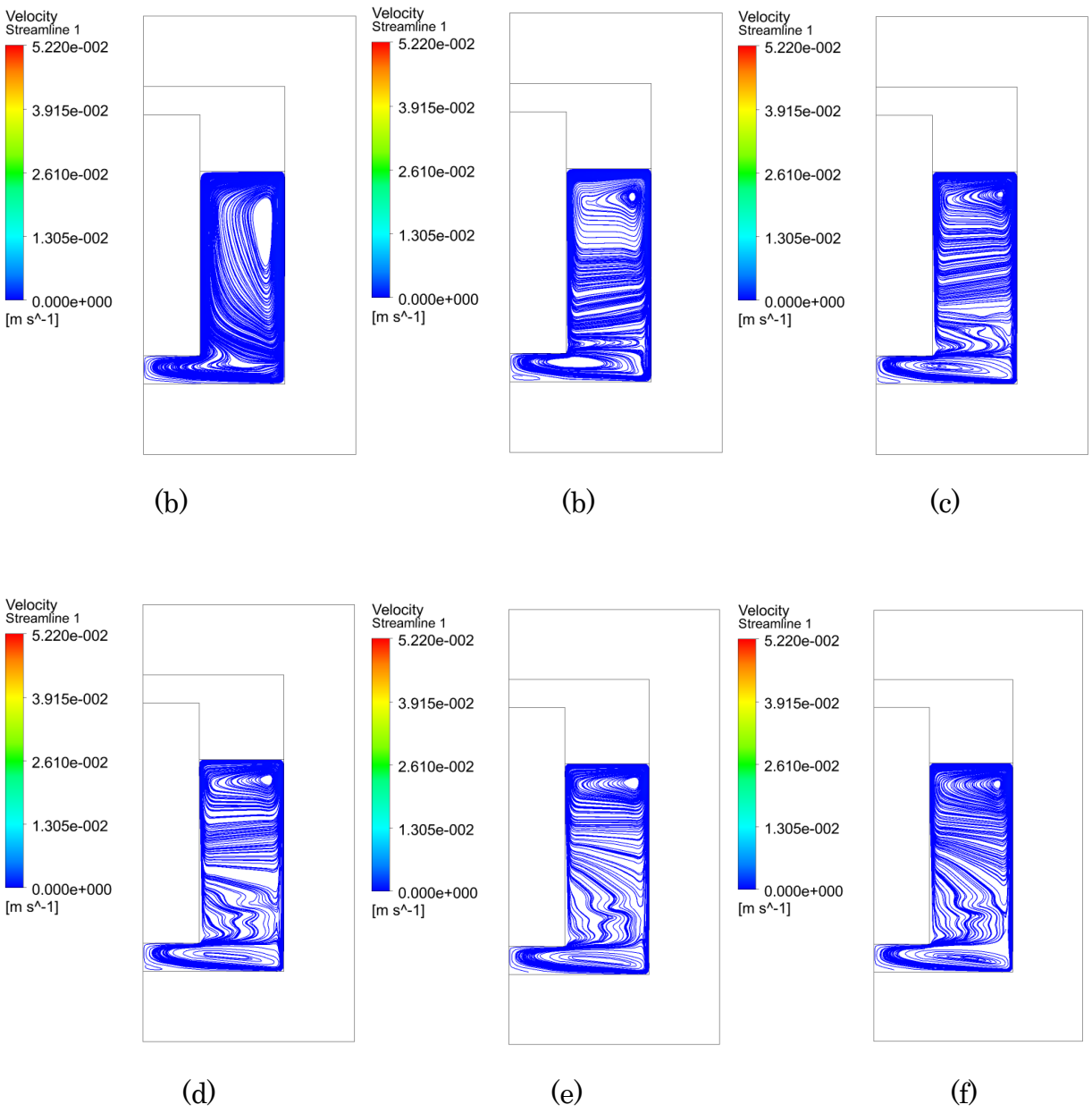

Figure 4.16: Flow streamlines in the biodiesel at different times between the phase change process from liquid to solid: (a) t = 1 hr, (b) t = 25 hrs, (c) t = 50 hrs, (d) t = 63 hrs, (e) t = 70 hrs, and (f) t = 72 hrs.

5

Conclusions and recommendations

This research work presents a 1-D numerical model which is validated by comparison with experimental results. The results indicate that the long-term average temperature of the fuel tank can be predicted with good accuracy without the imminent need to use more sophisticated CFD software. This significantly saves simulation time and is helpful to give insight on the 'big picture' while evaluating tank performance. CFD software like ANSYS can be used to conduct a more detailed study as the sample case which was presented in the study. However, tanks implementing PCM can have complex designs and an accurate study may not be possible without conducting a large-scale 3D simulation. This would usually require large number of nodes and huge computational power because of the complex phenomena of phase change, heat transfer and fluid flow that must be solved numerically.

Consequently, the solution to the complex problem has been simplified by only having the knowledge of the tank overall heat transfer coefficient, heat loss area, properties of the oil and PCM, the submerged depth of the PCM and the number of PCM pencils. As earlier highlighted, this method can be directly applicable to B100 biodiesels since they are believed to exhibit similar thermal behaviours to other Newtonian fluids at temperatures above cloud point where crystallization begins.

Evidently, the hypothesis that PCMs can be used in biodiesel tank design to extend the time above cloud point has been justified both experimentally and numerically. The following points summarize the results obtained from the analysis conducted for tank designs with the PCM pencils:

1. The heat transfer between the PCM and the oil depends strongly on the wetted contact area. Therefore, the PCM can be utilized more effectively by a tank design where the contact is maximized for most storage scenarios.
2. Increasing the number of PCM pencils increases the time above cloud point linearly, however, it reduces the overall tank capacity due to the space occupied by the pencils.
3. Increasing or decreasing the PCM pencil's diameter has no overall effect in the long-term on the time the oil stays above cloud point. The differences in the oil temperatures were only observed during the phase change period primarily due to the variation in contact area for transfer of stored latent heat.
4. The overall heat transfer coefficient appears to have a significant impact on the tank performance. Given that the insulation contributes to the highest

thermal resistance, the tank performance could be improved by using a better insulation technique and an insulation with very low thermal conductivity and larger thickness. For more compact designs, vacuum insulated panels (VIP) could be considered.

5. Increasing the filling level or volume of oil in the tank also improves the time above cloud point because more PCM is involved in the heat transfer process, but there appears to be a limit on the improvement that can be obtained when compared with tanks without PCM. This could be a result of the increased heat loss area as the volume of oil in the tank increases.
6. Detailed analysis using ANSYS Fluent indicates that the thermal stratification in the oil due to heat loss by natural convection would ultimately result in clouding beginning at the bottom of the tank which could potentially pose a problem in operation.

Remember that an assumed initial temperature of 20°C have been used in all the cases discussed to illustrate the concept, however, in real scenarios, the biodiesel should be heated to as high as 40°C which would further extend the time above cloud point. While this technology may not easily attain large scale adoption due to current cost of B100 biodiesel and availability, it can be an attractive option to entrepreneurs and farmers who seek to operate net-zero by producing all the energy they consume, thereby reducing their GHG emissions and potentially selling carbon credits for more income. The concept can be readily adapted to an existing truck fuel tank or entirely

new custom tank design and connected to the compression ignition engine as discussed in Section 1.12.

5.1 Recommendations for future work

The visualization study conducted on the sample case using ANSYS Fluent indicate that the process of solidification of the PCM begins in the upper portion of the tube because of the exposure to air which is at a lower temperature due to its lower specific heat capacity. Therefore, a significant portion of the latent heat in the PCM is not effectively used to preserve the temperature of the B100 biodiesel above cloud point for longer periods since it is lost to the surrounding air. An alternative design could be considered whereby the PCM pencils are positioned in a way to maximize contact with the oil irrespective of the filling level of the tank. A good method might be using spherical encapsulated low temperature PCM which forms a bed just below the exit port of the tank as show in Figure 5.1, resulting in any latent energy being stored being utilized by the biodiesel only.

Another method could involve fabricating a custom tank which contains many shorter PCM pencils so contact could be maximized until at least the fuel level goes below 25%. However, this takes away the advantage of having the PCM pencils removeable as the current design proposes.

To address the problem of local crystallization beginning at the bottom of the tank using PCM pencils, future designs can make the PCM pencils extend closer to the

base of the tank so that the biodiesel in the lower part of the tank receive more latent energy.

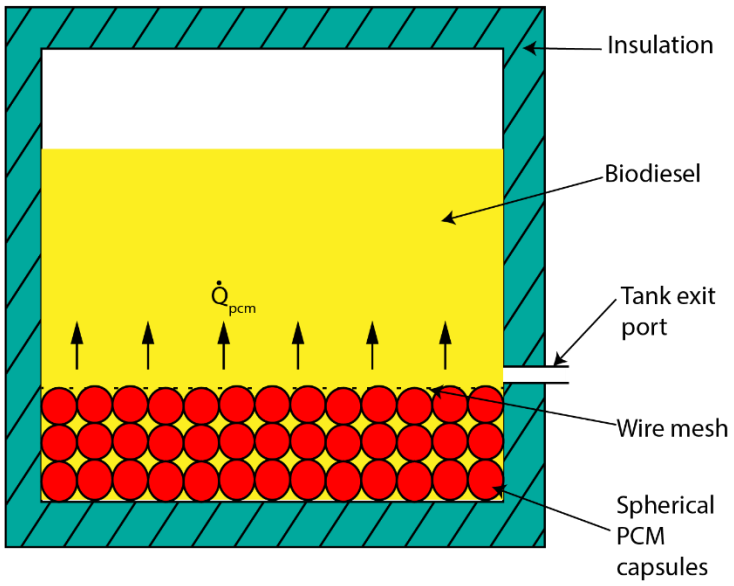

Figure 5.1: Conceptual biodiesel tank design using spherical encapsulated PCM

Figure 4.13(b) demonstrates this as the highest temperature gradient can be observed just below the PCM tube. The use of spherical encapsulated PCM which sits at the base of the tank as earlier highlighted or a custom base with PCM lining could also potentially address this issue. It is also recommended to have a fuel exit port at a location other than the base of the tank to prevent clogging of the fuel line.

While this research focuses primarily on the design of the tanks for use of B100 biodiesel in winter, further work needs to be done to investigate ways in which PCM could also be implemented in fuel lines to prevent freezing. A possible solution could be having a fuel line design with concentric PCM and insulation layers and an electric heating backup. As an alternative approach, the fuel line problem could be solved by

implementing the design alongside petroleum diesel in a heavy-duty truck to prevent start-up problems. In this scenario, one of the fuel tanks would contain petroleum diesel, while the other tank with the PCM design would contain B100. Due to the lower cloud point of petroleum diesel, the engine would be started up with fuel coming from the petroleum diesel tank only. As the engine and the fuel line gets warmer, B100 can be gradually introduced to the engine until it completely takes over and the petroleum diesel supply is shut off.

Finally, further research is still needed on producing low-temperature PCM with higher latent energy storage capacity to give this proposed design a greater and commercial adoption.

Bibliography

[1] Population Reference Bureau, "2016 World Population Data Sheet," *2015 World Popul. Data Sheet*, p. 23, 2016.

[2] U. S. Energy, "International Energy Outlook 2017 Overview," *Int. Energy Outlook*, vol. IEO2017, no. 2017, p. 143, 2017.

[3] British Petroleum, "BP Statistical Review of World Energy 2017," *Br. Pet.*, no. 66, pp. 1–52, 2017.

[4] E. P. Agency, "Atmospheric Concentrations of Greenhouse Gases," no. August, pp. 1–13, 2016.

[5] W. R. Chang, J. J. Hwang, and W. Wu, "Environmental impact and sustainability study on biofuels for transportation applications," *Renew. Sustain. Energy Rev.*, vol. 67, pp. 277–288, 2017.

[6] Y. Su, P. Zhang, and Y. Su, "An overview of biofuels policies and industrialization in the major biofuel producing countries," *Renew. Sustain. Energy Rev.*, vol. 50, pp. 991–1003, 2015.

[7] "Clean Cities Alternative Fuel Price Report," 2017.

[8] ASTM, *ASTM D6751-02, Standard Specification for Biodiesel Fuel (B100) Blend Stock for Distillate Fuels*. West Conshohocken, PA, 2002.

[9] T. L. Alleman, R. L. McCormick, E. D. Christensen, G. Fioroni, K. Moriarty, and J. Yanowitz, *Biodiesel Handling and Use Guide*, no. November. 2016.

[10] O. Edith, B. J. Rimfiel, and Y. Robiah, "Factors affecting the cold flow behaviour of biodiesel and methods for improvement - A review," *Pertanika J. Sci. Technol.*, vol. 20, no. 1, pp. 1–14, 2012.

[11] Graydon Blair, "Running Biodiesel In The Cold - Utah Biodiesel Supply Blog," 2012. [Online]. Available: http://www.utahbiodieselsupply.com/blog/running-biodiesel-in-the-cold/. [Accessed: 27-Nov-2017].

[12] M. M. K. Bhuiya, M. G. Rasul, M. M. K. Khan, N. Ashwath, A. K. Azad, and M. A. Hazrat, "Prospects of 2nd generation biodiesel as a sustainable fuel - Part 2: Properties, performance and emission characteristics," *Renew. Sustain. Energy Rev.*, vol. 55, pp. 1129–1146, 2016.

[13] A. E. Atabani, A. S. Silitonga, I. Anjum, T. M. I. Mahlia, H. H. Masjuki, and S. Mekhilef, "A comprehensive review on biodiesel as an alternative energy resource and its characteristics," *Renew. Sustain. Energy Rev.*, vol. 16, no. 4, pp. 2070–2093, 2012.

[14] R. O. Dunn, M. W. Shockley, and M. O. Bagby, "Improving the low-temperature properties of alternative diesel fuels: vegetable oil-derived methyl esters," *J Am Oil Chem Soc*, vol. 73, no. 12, pp. 1719–28, 1996.

[15] H. Lin, D. M. Haagenson, D. P. Wiesenborn, and S. W. Pryor, "Effect of trace contaminants on cold soak filterability of canola biodiesel," *Fuel*, vol. 90, no. 5, pp. 1771–1777, 2011.

[16] J. F. Sierra-Cantor and C. A. Guerrero-Fajardo, "Methods for improving the

cold flow properties of biodiesel with high saturated fatty acids content: A review," *Renew. Sustain. Energy Rev.*, vol. 72, no. April 2016, pp. 774–790, 2017.

[17] R. O. Dunn and M. O. Bagby, "Low-temperature properties of triglyceride-based diesel fuels: Transesterified methyl esters and petroleum middle distillate/ester blends," *J. Am. Oil Chem. Soc.*, vol. 72, no. 8, pp. 895–904, 1995.

[18] C. C. C. Bejan, V. G. Celante, E. Vinicius Ribeiro De Castro, and V. M. D. Pasa, "Effect of different alcohols and palm and palm kernel (palmist) oils on biofuel properties for special uses," *Energy and Fuels*, vol. 28, no. 8, pp. 5128–5135, 2014.

[19] P. C. Smith, Y. Ngothai, Q. D. Nguyen, and B. K. O. Neill, "Improving the low-temperature properties of biodiesel : Methods and consequences," *Renew. Energy*, vol. 35, no. 6, pp. 1145–1151, 2010.

[20] G. Knothe, "Dependence of biodiesel fuel properties on the structure of fatty acid alkyl esters," *Fuel Process. Technol.*, vol. 86, no. 10, pp. 1059–1070, 2005.

[21] R. D. Misra and M. S. Murthy, "Blending of additives with biodiesels to improve the cold flow properties, combustion and emission performance in a compression ignition engine - A review," *Renew. Sustain. Energy Rev.*, vol. 15, no. 5, pp. 2413–2422, 2011.

[22] T. Q. Chastek, "Improving cold flow properties of canola-based biodiesel," *Biomass and Bioenergy*, vol. 35, no. 1, pp. 600–607, 2011.

[23] C. W. Chiu, L. G. Schumacher, and G. J. Suppes, "Impact of cold flow improvers on soybean biodiesel blend," *Biomass and Bioenergy*, vol. 27, no. 5, pp. 485–491, 2004.

[24] G. Dwivedi and M. P. Sharma, "Investigation of Cold Flow Properties of Waste Cooking Biodiesel," vol. 4, no. 3, 2016.

[25] A. Y. Benavides, P. N. Benjumea, and J. R. Agudelo, "Crystallization fractionation of palm oil biodiesel as an alternative for improving its cold flow properties ," *El fraccionamiento por Cristal. del biodiesel aceite palma como Altern. para Mejor. sus propiedades flujo a baja Temp.*, no. March, pp. 7–17, 2008.

[26] "Warner Truck Center – Vince Stinson UXUI Designer and more." [Online]. Available: http://www.vincestinson.com/portfolio/warner/. [Accessed: 17-Apr-2018].

[27] "OEM Warranty Statements and Use of Biodiesel Blends over 5% (B5)," *National Biodiesel Board*. [Online]. Available: http://biodiesel.org/docs/default-source/ffs-engine_manufacturers/oem-warranty-statement-and-use-of-biodiesel-blends-over-5-(b5).pdf?sfvrsn=6. [Accessed: 24-Nov-2017].

[28] L. F. Cabeza, *Advances in thermal energy storage systems : methods and applications*. Elsevier Science & Technology, 2014.

[29] F. J. Rentas, V. W. Macdonalds, D. W. Houchens, P. J. Hmel, and T. J. Reid, "New insulation technology provides next generation containers for 'iceless' and

lightweight transport of RBC's at 1 to 10 degrees C in extreme temperatures for over 78 hours," *Transfusion*, vol. 44, pp. 210–2016, 2004.

[30] S. D. Sharma and K. Sagara, "Latent Heat Storage Materials and Systems: A Review," *Int. J. Green Energy*, vol. 2, no. 1, pp. 1–56, Jan. 2005.

[31] K. Wojciechowski, J. Merkisz, P. Fuć, P. Lijewski, and M. Schmidt, "Study of Recovery of Waste Heat from the Exhaust of Automotive Engine," *5th Eur. Conf. Thermoelectr.*, 2007.

[32] P. Kauranen, T. Elonen, L. Wikstr??m, J. Heikkinen, and J. Laurikko, "Temperature optimisation of a diesel engine using exhaust gas heat recovery and thermal energy storage (diesel engine with thermal energy storage)," *Appl. Therm. Eng.*, vol. 30, no. 6–7, pp. 631–638, 2010.

[33] M. Gumus, "Reducing cold-start emission from internal combustion engines by means of thermal energy storage system," *Appl. Therm. Eng.*, vol. 29, no. 4, pp. 652–660, 2009.

[34] "Electricity price statistics," *Eurostat*, 2017. [Online]. Available: http://ec.europa.eu/eurostat/statistics-explained/index.php/Electricity_price_statistics. [Accessed: 24-Nov-2017].

[35] D. Roberts, "The world's largest car market just announced an imminent end to gas and diesel cars - Vox," *Vox*, 2017. [Online]. Available: https://www.vox.com/energy-and-environment/2017/9/13/16293258/ev-revolution. [Accessed: 24-Nov-2017].

[36] C. Rauwald, "VW to Roll Out Electric Trucks, Buses in $1.7 Billion Push," *Bloomberg*, 2017. [Online]. Available: https://www.bloomberg.com/news/articles/2017-10-11/vw-to-roll-out-electric-trucks-buses-in-1-7-billion-project. [Accessed: 24-Nov-2017].

[37] "B100 Materials Compatibility," *National Biodiesel Board*. [Online]. Available: http://biodiesel.org/docs/ffs-performace_usage/materials-compatibility.pdf. [Accessed: 24-Nov-2017].

[38] A. I. Fernández, C. Barreneche, L. Miró, S. Brückner, and L. F. Cabeza, "Thermal energy storage (TES) systems using heat from waste," *Adv. Therm. Energy Storage Syst.*, pp. 479–492, 2015.

[39] J. Bailey, "Modelling Phase Change Material Thermal Storage Systems," McMaster University, 2010.

[40] L. Miro, C. Barreneche, S. Bruckner, A. I. Fernández, and L. F. Cabeza, "Recovering waste heat using thermal energy storage technologies," in *Proceedings from Eurotherm Seminar #99: Advances in Thermal Energy Storage.*, 2014.

[41] H. Mehling and L. F. Cabeza, *Heat and Cold Storage with PCM: An Up to Date Introduction into Basics and Applications*. Heidelberg, Berlin: Springer, 2008.

[42] A. Gil *et al.*, "State of the art on high temperature thermal energy storage for power generation. Part 1—Concepts, materials and modellization," *Renew. Sustain. Energy Rev.*, vol. 14, no. 1, pp. 31–55, 2010.

[43] C. Prieto, P. Cooper, A. I. Fernández, and L. F. Cabeza, "Review of technology: Thermochemical energy storage for concentrated solar power plants," *Renew. Sustain. Energy Rev.*, vol. 60, pp. 909–929, 2016.

[44] Arcon Sunmark, "Seasonal heat storage boosting the effect of the world's largest solar heating plant." [Online]. Available: http://arcon-sunmark.com/cases/vojens-district-heating. [Accessed: 16-Mar-2018].

[45] Z. Khan, Z. Khan, and A. Ghafoor, "A review of performance enhancement of PCM based latent heat storage system within the context of materials, thermal stability and compatibility," *Energy Convers. Manag.*, vol. 115, pp. 132–158, 2016.

[46] Y. Lin, Y. Jia, G. Alva, and G. Fang, "Review on thermal conductivity enhancement, thermal properties and applications of phase change materials in thermal energy storage," *Renew. Sustain. Energy Rev.*, vol. 82, no. September 2017, pp. 2730–2742, 2018.

[47] H. Yin, X. Gao, J. Ding, and Z. Zhang, "Experimental research on heat transfer mechanism of heat sink with composite phase change materials," *Energy Convers. Manag.*, vol. 49, no. 6, pp. 1740–1746, 2008.

[48] L. F. Cabeza *et al.*, "Immersion corrosion tests on metal-salt hydrate pairs used for latent heat storage in the 32 to 36 C temperature range," *Werkstoffe und Korrosion*, vol. 52, no. 2, pp. 140–146, 2001.

[49] K. Kaygusuz, "Experimental and Theoretical Investigation of Latent-heat

Storage For Water-based Solar Heating-systems," *Energy Convers. Manag.*, vol. 36, no. 5, pp. 315–323, 1995.

[50] N. I. Ibrahim, F. A. Al-Sulaiman, S. Rahman, B. S. Yilbas, and A. Z. Sahin, "Heat transfer enhancement of phase change materials for thermal energy storage applications: A critical review," *Renew. Sustain. Energy Rev.*, vol. 74, no. February, pp. 26–50, 2017.

[51] L. Shilei, Z. Neng, and F. Guohui, "Impact of phase change wall room on indoor thermal environment in winter," vol. 38, pp. 18–24, 2006.

[52] S. Canbazoğlu, A. Şahinaslan, A. Ekmekyapar, Y. G. Aksoy, and F. Akarsu, "Enhancement of solar thermal energy storage performance using sodium thiosulfate pentahydrate of a conventional solar water-heating system," *Energy Build.*, vol. 37, no. 3, pp. 235–242, 2005.

[53] A. Gadgil and D. Gobin, "Analysis of Two-Dimensional Melting in Rectangular Enclosures in Presence of Convection," *J. Heat Transfer*, vol. 106, no. 1, pp. 20–26, Feb. 1984.

[54] G. Ziskind, "12 - Modelling of heat transfer in phase change materials (PCMs) for thermal energy storage systems," in *Advances in Thermal Energy Storage Systems*, L. F. Cabeza, Ed. Woodhead Publishing, 2015, pp. 307–324.

[55] J. Stefan, "Uber einige probleme der theorie der warmeleitung," *S B Wien Akad. Mat. Natur.*, no. 98, pp. 473–484, 1889.

[56] H. Hu and S. a Argyropoulos, "Mathematical modelling of solidification and

melting: a review," *Model. Simul. Mater. Sci. Eng.*, vol. 4, no. 4, pp. 371–396, 1999.

[57] D. Poirier and M. Salcudean, "On numerical methods used in mathematical modeling of phase change in liquid metals," *ASME J. Heat Transf.*, vol. 110, pp. 562–570, 1988.

[58] J. Bony and S. Citherlet, "Numerical model and experimental validation of heat storage with phase change materials," *Energy Build.*, vol. 39, no. 10, pp. 1065–1072, 2007.

[59] H. Shmueli, G. Ziskind, and R. Letan, "Melting in a vertical cylindrical tube: Numerical investigation and comparison with experiments," *Int. J. Heat Mass Transf.*, vol. 53, no. 19–20, pp. 4082–4091, 2010.

[60] M. A. Cotter and M. E. Charles, "Transient cooling of petroleum by natural convection in cylindrical storage tanks: A simplified heat loss model," *Can. J. Chem. Eng.*, vol. 70, no. 6, pp. 1090–1093, Dec. 1992.

[61] C. Suárez, A. Iranzo, F. J. Pino, and J. Guerra, "Transient analysis of the cooling process of molten salt thermal storage tanks due to standby heat loss," *Appl. Energy*, vol. 142, pp. 56–65, 2015.

[62] M. A. Cotter and M. E. Charles, "Transient cooling of petroleum by natural convection in cylindrical storage tanks—I. Development and testing of a numerical simulator," *Int. J. Heat Mass Transf.*, vol. 36, no. 8, pp. 2165–2174, 1993.

[63] R. De Césaro Oliveski, M. H. MacAgnan, J. B. Copetti, and A. De La Martinière Petroll, "Natural convection in a tank of oil: Experimental validation of a numerical code with prescribed boundary condition," *Exp. Therm. Fluid Sci.*, vol. 29, no. 6, pp. 671–680, 2005.

[64] L. F. Cabeza, M. Ibáñez, C. Solé, J. Roca, and M. Nogués, "Experimentation with a water tank including a PCM module," *Sol. Energy Mater. Sol. Cells*, vol. 90, no. 9, pp. 1273–1282, 2006.

[65] A. S. Ramana, R. Venkatesh, V. Antony Aroul Raj, and R. Velraj, "Experimental investigation of the LHS system and comparison of the stratification performance with the SHS system using CFD simulation," *Sol. Energy*, vol. 103, pp. 378–389, 2014.

[66] G. S. Kumar, D. Nagarajan, L. A. Chidambaram, V. Kumaresan, Y. Ding, and R. Velraj, "Role of PCM addition on stratification behaviour in a thermal storage tank – An experimental study," *Energy*, vol. 115, pp. 1168–1178, 2016.

[67] Rubitherm, "RT18HC Data sheet." Rubitherm GmbH, 2016.

[68] S. W. Churchill and H. H. S. Chu, "Correlating equations for laminar and turbulent free convection from a vertical plate," *Int. J. Heat Mass Transf.*, vol. 18, no. 11, pp. 1323–1329, 1975.

[69] R. De Césaro Oliveski, A. Krenzinger, and H. A. Vielmo, "Cooling of cylindrical vertical tanks submitted to natural internal convection," *Int. J. Heat Mass Transf.*, vol. 46, no. 11, pp. 2015–2026, 2003.

[70] J. Bony and S. Citherlet, "Extension of a TRNSYS model for latent heat storage with phase change materials used in solar water tank," *Ecostock2006, Stock.*, no. 1, 2006.

[71] T. L. Bergman, A. S. Lavine, and F. P. Incropera, *Fundamentals of Heat and Mass Transfer, 7th Edition*. John Wiley & Sons, Incorporated, 2011.

[72] R. Przybylski, "Canola Oil: Physical and Chemical Properties," *Canola Counc. Canada*, pp. 1–6, 2011.

[73] R. De Césaro Oliveski, "Correlation for the cooling process of vertical storage tanks under natural convection for high Prandtl number," *Int. J. Heat Mass Transf.*, vol. 57, no. 1, pp. 292–298, 2013.

[74] D. Q. Santos, A. L. De Lima, A. P. De Lima, W. B. Neto, and J. D. Fabris, "Thermal expansion coefficient and algebraic models to correct values of specific mass as a function of temperature for corn biodiesel," *Fuel*, vol. 106, pp. 646–650, 2013.